Schultz, A., Orcutt, J.A., and Davies, T.A. (Eds.)
Proceedings of the Ocean Drilling Program, Scientific Results Volume 203

2. Enriched, Transitional, and Normal Mid-Ocean-Ridge Basaltic Glass, ODP Leg 203[1]

R. Moberly,[2] T. Ishii,[3] M.O. Garcia,[2,4] K. Ross,[2] and K. Artita[2,5]

ABSTRACT

Sand-sized basaltic glass fragments were recovered in the liner of Core 203-1243B-19R, the deepest recovery from Hole 1243B. Microprobe analysis of 582 glassy cuttings cluster into five compositionally distinct groups, most of which are unlike the lithologic units described on board ship. Drilling operations intended to sweep cuttings from the caving hole and differences between the cuttings and geochemically distinct lithologic units of the upper part of the basement indicate that the cuttings came mainly, if not entirely, from the lower part of the hole. They give information about the part of Hole 1243B that had poor core recovery. Enriched mid-ocean-ridge basalt (MORB) from the upper part of the hole and transitional MORB from two groups of cuttings from sources low in the hole may be a trace of the Galápagos plume on the Pacific plate or may be a normal consequence of eruptions from two distinct magmas on fast-spreading crust.

INTRODUCTION

The purpose of Ocean Drilling Program Leg 203 was to drill and case into basement a reentry hole in the eastern Pacific as a legacy for a future multidisciplinary observatory for the Dynamics of Earth and Ocean Systems Program. To optimize the potential value as a seismic and oceanographic observatory, Site 1243 (5°18.0541′N, 110°4.5798′W) was selected for its position relative to the Middle America seismic belt and East Pacific Rise and within the near-equatorial circulation system.

[1] Moberly, R., Ishii, T., Garcia, M.O., Ross, K., and Artita, K., 2006. Enriched, transitional, and normal mid-ocean-ridge basalt glass, ODP Leg 203. *In* Schultz, A., Orcutt, J.A., and Davies, T.A. (Eds.), *Proc. ODP, Sci. Results,* 203, 1–36 [Online]. Available from World Wide Web: <http://www-odp.tamu.edu/publications/203_SR/VOLUME/CHAPTERS/002.PDF>. [Cited YYYY-MM-DD]
[2] Department of Geology and Geophysics, School of Ocean and Earth Science and Technology, University of Hawaii at Manoa, 1680 East-West Road, Honolulu HI 96822, USA. Correspondence author: **ralph@soest.hawaii.edu**
[3] Ocean Research Institute, University of Tokyo, 1-15-1 Minamidai, Nakano-ku, Tokyo 164-8639, Japan.
[4] Present address: University of California, 307 McCone Hall, Berkeley CA 94720, USA.
[5] Present address: 315-3 Union Hill Road, Carbondale IL 62903, USA.

Initial receipt: 26 May 2005
Acceptance: 1 February 2006
Web publication: 21 September 2006
Ms 203SR-002

Other factors contributing to the selection of this site were the opportunity to sample fast-spreading crust (full spreading rate = ~140 mm/yr) of moderately young age (~ 10 Ma) for geochemistry, the anticipated alteration of that crust, the time saved by drilling rather than coring the sedimentary section known from adjacent Site 852 cored earlier, and the time available for drilling and transit.

Hole 1243A was drilled and cased for future instrumentation, and adjacent Hole 1243B was drilled through the sedimentary section in order to core oceanic crust. Top of basement in Hole 1243B was determined to be at 108.2 meters below the seafloor (mbsf), and the hole was then cored to a total depth of 195.3 mbsf, penetrating 87.1 m of uppermost oceanic crust. Depths from wireline logging were 6.3 m deeper, requiring caution when comparing logs and cores. This present report on composition of glass uses the core depths that came from measurements of the drill pipe, termed the curated depths. Average recovery was 24.8% and was better in the upper Cores 203-1243B-2R through 10R (34.8%) than in the lower Cores 203-1243B-11R through 18R (15.1%). The three deepest cores each recovered <10% of the penetrated interval. The lower part of the hole had extensive caving that led to severe operational problems, including high torque and loss of rotation, plugging of the core catcher, and filling the bottom of the hole between coring runs. Twice the hole packed off, requiring overpull of the drill string and higher pump strokes. Sepiolite mud was swept after each core to clear the hole. The two caliper logs show extensive caving below ~156 mbsf (Core 203-1243B-11R and deeper), as confirmed by decreases in wireline-logged resistivity, sonic velocity, and bulk density. As a result, when the leg ended, the bottom of Hole 1243B remained virtually unknown.

Recovered rock was divided into eight basement units (Fig. F1) on the basis of shipboard visual examination of phenocryst content, vesicularity, and degree of alteration. Of particular interest is Unit 4, an alkalic basalt.

F1. Basement section, p. 12.

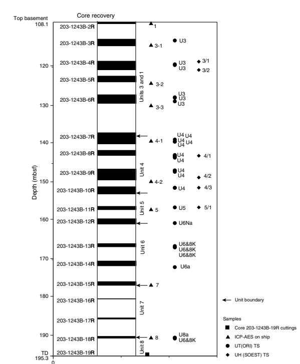

Core 203-1243B-19R, the lowermost "core" of Hole 1243B, consisted of 5.3 m of millimeter- and submillimeter-sized fragments or chips of basalt and basalt glass. The fragments in the core barrel liner represented cuttings and cavings that had not been washed from the hole. Although termed a drilling breccia in figure F11 in the "Site 1243" chapter of the Leg 203 *Initial Reports* (Shipboard Scientific Party, 2003b), these angular sand-sized particles do not constitute a breccia, which is a solid rock of angular fragments coarser than sand in size.

METHODS AND MATERIALS

It was proposed that numerous analyses of glass from the cuttings might provide geochemical information about the interval from which recovery was poor and perhaps even provide some "average" sampling of the composition for the upper part of the oceanic crust at Site 1243. This idea assumes that all lithologic units were equally brittle, the ratio of glass to hypocrystalline basalt is comparable for all units, and the cuttings had been sufficiently churned so that a random sampling of the recovered cuttings would be a random sample of the drilled interval.

A few dozen glassy-appearing fragments were picked from the exposed sections, and several scoops of 10–20 cm^3 were taken at random from all core liner sections. The sampled material taken ashore was assumed to be a random representation of the cuttings, as there was no layering or grading of the fragments in the core liners. From several thousand grains examined under a binocular microscope, most of which proved to be hypocrystalline, ~600 glassy grains were picked and mounted in epoxy plugs and then ground, polished, and coated for microprobe analysis. Under the electron microprobe, some chips were too small or altered for analysis or contained abundant microlites. Nevertheless, 582 glassy grains of ~1.0–2.5 mm diameter were analyzed; 580 with 4 analyses each, and 2 with 3 analyses each, totaling 2326 analyses. The data presented here are arithmetic means of the analyses of these 582 samples (Table **T1**).

T1. Basaltic glass composition, p. 28.

Nine pieces of core with glassy pillow edges were sampled as thin sections for analysis at the School of Ocean and Earth Sciences and Technology (SOEST), University of Hawaii (USA). Analyses of the glasses provide additional information for certain shipboard-defined basalt units and thereby allow lithologic comparison and correlation between cuttings and the stratigraphy of the cored interval. Upon petrographic examination, three samples proved to be heavily altered, but six sections with fresh to barely altered glass were polished and coated for microprobe analysis (Table **T2**).

T2. Thin section analyses, p. 29.

Cuttings and thin sections were analyzed at SOEST using a CAMECA SX-50 electron microprobe. The instrument was operated with electron beam energy of 15 kV and beam current of 15 nA. The electron beam was rastered over a region of ~15 µm × 10 µm in order to minimize beam-induced damage to the specimen and Na loss. The major elements were calibrated on U.S. National Museum glass standards Juan de Fuca VG2 (Ca, Al, and Mg) and Makaopuhi A99 (Si, Fe, Ti, and Na). Minor elements were calibrated using apatite (P), verma garnet (Mn), and orthoclase (K). Count times were generally 30 s on peaks, with 15 s on high- and low-background offsets. Calibration and instrumental drift were monitored by checking results on standards before and after automated analytical runs. Elements are converted to oxides, with total Fe given as FeO. As will be shown, tightness of groupings of analyses of the cuttings suggests the analytical error is approximately the range of the values within a group (Fig. **F2**).

F2. MgO vs. K_2O/TiO_2, p. 13.

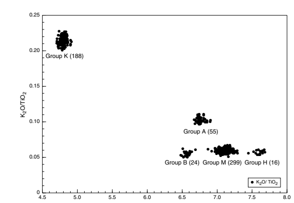

Additional samples analyzed at Ocean Research Institute (ORI), University of Tokyo (Japan), are reported here only in preliminary form (Table **T3**).

T3. Raw microprobe data, p. 30.

Composition of Glass from Cuttings

First, we show that the glass cuttings fall into only a few compositional groups. We present the geochemical characteristics for those groups as evidence for their distinctness. Next, we compare the compositions of the cuttings with compositions from samples from known stratigraphic intervals in the hole and conclude that the cuttings come predominantly if not entirely from the lower part of the hole, from which core recovery was minimal. Lastly, we use geochemical information from cuttings and cores to relate mid-ocean-ridge basalt (MORB) of Site 1243 with MORB of spreading centers in the eastern Pacific.

Examination of TiO_2, K_2O, Al_2O_3, FeO, K_2O/TiO_2, and other components and ratios of the 582 analyzed samples of Leg 203 glass fragments showed that the analyses cluster into five geochemical groupings (Table **T4**). For the purposes of this report, the groups are named as follows. Group M, the main group, contains 299 samples. The second largest group, with 188 samples, is Group K, named for its high K_2O content.

T4. Geochemical groups, p. 34.

Group K is also high in FeO, P_2O_5, Na_2O, and TiO_2, and FeO/CaO is ~1.3. Certain samples with similar TiO_2 contents separate into two groups when other oxides (e.g., Al_2O_3 or FeO) were considered, so that on certain graphs Group A (55 samples) plotted above and Group B (24 samples) plotted below one another. FeO/CaO is slightly <1.0 for Group A but slightly >1.0 for Group B. Group H (16 samples) has the highest MgO; low FeO, Na_2O, and P_2O_5; and lowest K_2O and TiO_2 contents.

A method commonly used to indicate possible consanguinity of mafic igneous rocks is to compare magnesium content to the ratio of potassium to titanium (Cushman et al., 2004, and references therein) (K/Ti = $K_2O/TiO_2 \times 0.706$). Variation in MgO for constant K_2O/TiO_2 would suggest modest differentiation in lavas from a common parental basaltic reservoir. Figure F2, showing the five groups of Leg 203 glass samples, indicates that Groups K and A are clearly separate but that Group M might be related to Groups B and H with variation in MgO content.

Most Leg 203 glass-fragment compositions fall in the tholeiitic field of Macdonald and Katsura (1964). Some of the Leg 203 glasses, however, plot near or slightly above the dividing line and are termed transitional and alkalic basalts (Fig. F3). Averages for normal (N)-type and enriched (E)-type MORB, according to McBirney (1993), are shown on this and several other figures and in Table T5. Of the five groups of Leg 203 glass, high-K Group K is highest in total alkalis but there is a wide scatter in the data. Group A is moderately distinct, whereas groups B and H merge into the upper and lower bounds, respectively, of Group M. Note that the average for N-MORB is in the middle of the Group M analyses, whereas average E-MORB lies distinctly below Group K and somewhat above Group A.

The K_2O content of average N-MORB is nearly double the K_2O of glasses in Groups B, M, and H (Fig. F4). The scatter of $Na_2O + K_2O$ in Groups K and M of Figure F3 is shown to be scatter in Na_2O, probably from incipient alteration of the glasses. The K_2O content of average E-MORB is distinctly less than K_2O in Group K. In reporting their work along the Galápagos spreading center, Cushman et al. (2004) defined the lower boundary for E-MORB as 0.2 wt% K_2O content and a 0.15 K/Ti ratio. Group A is borderline E-MORB on the first criterion but is N-MORB on K/Ti.

The compatible major elements Mg, Al, Ca, and Fe are plotted as oxides in Figure F5. With increased MgO there is a general increase in Al_2O_3 and a slight increase in CaO, but there is a decrease in total Fe as FeO (Fig. F5). With its MgO at ~7.5%, average N-MORB lies between Groups H and M but plots slightly higher for Al_2O_3 and lower for CaO. Average E-MORB lies at the edge of the Group A fields for the three oxides. The CaO values plot in somewhat tighter clusters than values for Al_2O_3 and FeO, as shown in Figure F6, which magnifies the plot of Figure F5 for Groups B, A, M, and H. Group M, with 299 samples and approximately three times the number of Groups A, B, and H combined, has several samples with values of Al_2O_3 and FeO scattered below the principal clustering.

Certain additional points about the composition of the groups are revealed when Al_2O_3, CaO, FeO, and MgO are plotted against TiO_2. With increasing TiO_2 content as far as Group K (3 wt% TiO_2), Al_2O_3, CaO, and MgO decrease but FeO increases (Fig. F7). With the apparent split in values of Al_2O_3 and FeO (~2.0 wt%), TiO_2 is seen clearly in Figure F8, which is the part of Figure F7 near 2.0 wt% TiO_2. Analyses of Groups A

F3. Silica vs. total alkalies, p. 14.

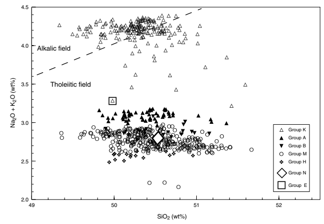

T5. Basalt composition averages, p. 35.

F4. SiO_2 vs. K_2O, p. 15.

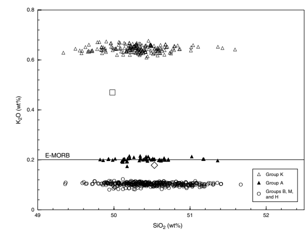

F5. MgO vs. Al_2O_3, CaO, and FeO, p. 16.

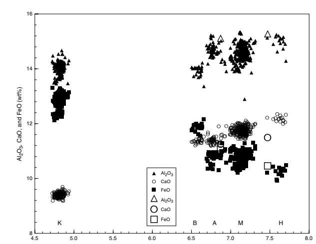

F6. Detail of MgO vs. Al_2O_3, CaO, and FeO, p. 17.

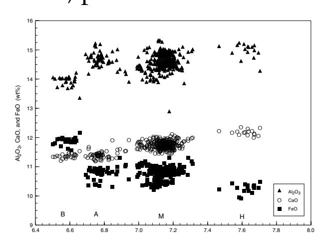

F7. TiO_2 vs. Al_2O_3, CaO, FeO, and MgO, p. 18.

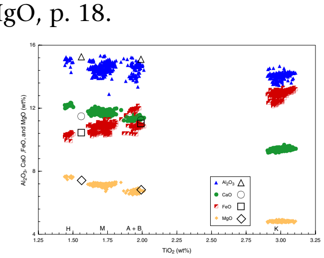

and B are plotted separately. Differences between Groups A and B are distinct in terms of Al_2O_3 and FeO, moderate in MgO, but not evident in CaO.

It is clear that five groups compose the glass cuttings. It is possible that two of the groups, M and K, have subgroups, perhaps from eruptions of multiple flow units that differed slightly in composition. A gap in the iron content of Group M is at ~10.6 wt% FeO, and there is a gap in iron content of Group K at ~ 12.5 wt% FeO. These gaps are also revealed in plots of S, K_2O, and P_2O_5 against FeO (Fig. F9). This diagram also shows the enrichment of K and P in Group K. The gaps are also apparent in the components at higher concentrations of Al_2O_3, CaO, and MgO plotted against FeO (Fig. F10).

The results of this microprobe work at University of Hawaii on glass from the cuttings and Figures F2 through F10 can be summarized as follows:

1. All analyses of glass fragments fall into only five relatively tight groupings, which strongly suggests that there are only five sources of the glass recovered from the cuttings at the bottom of Hole 1243B.
2. If the glass fragments analyzed represent a valid random sampling of the glass selvedges of the basalt flows' source section that was cored and if the proportion of glass to the interiors of the flows is similar from one flow to the next, this microprobe data set would indicate that the source of the basalt glass cuttings is approximately

   a. 51.4% (±2.0%) tholeiitic N-MORB: Group M;
   b. 2.7% (±0.6%) MORB resembling Group M but with higher Mg, Al, and Ca and lower Fe and Ti: Group H;
   c. 4.1% (±0.7%) MORB resembling Group M but with lower Mg, Al, and Ca and higher Fe and Ti: Group B;
   d. 9.4% (±1.2%) MORB resembling Group B in Ca and Ti content but differing in higher Fe, P, and K so as to be borderline enriched: Group A; and
   e. 32.3% (±1.8%) borderline alkalic, moderately enriched MORB: Group K.

Correlation with Units Defined On Board Ship

Groups of microprobe analyses either do not correlate with stratigraphic units (or parts of units) identified by shipboard petrographers or correlate tentatively with only a few units. This lack of matches indicates that the glass fragments are not a random sampling of the entire section drilled. Rather, they came largely, if not entirely, from the lower part of the hole, as expected because during continuous circulation, cuttings from higher, earlier-drilled units would have had a longer opportunity to be elutriated up the annulus than lower and later cuttings. As pointed out above, the drilling operations were designed to sweep out as much of the cuttings and cavings as possible.

Three sets of geochemical information from known stratigraphic positions are from (1) shipboard petrographic examination and geochemical analyses, (2) a set of uncorrected microprobe data of glass analyzed at ORI, and (3) microprobe analyses at SOEST of glass in thin sections. In comparing these SOEST microprobe analyses with those of ORI and the shipboard inductively coupled plasma–atomic emission spectroscopy

F8. Detail of TiO_2 vs. Al_2O_3, CaO, FeO, and MgO, p. 19.

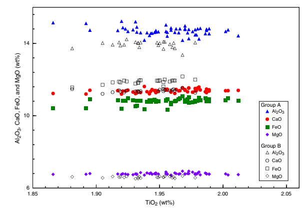

F9. FeO vs. S, K_2O, and P_2O_5, p. 20.

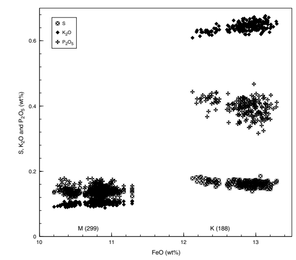

F10. FeO vs. Al_2O_3, CaO, and MgO, p. 21.

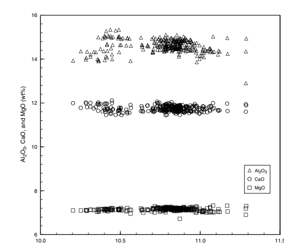

(ICP-AES) analyses, we bear in mind the caveat that ICP-AES whole-rock analyses are of pillow interiors, whereas probe analyses are of glass.

Division of the basement section into eight units, as initially defined (Shipboard Scientific Party, 2003a), requires a few comments. Unit 2, ~1 or 2 m below the top of basement, is not basalt. It is a 2-cm-thick piece of palagonite- and peloid-bearing foraminiferal limestone. It represents calcareous ooze that drifted into a fissure in the irregular surface of the last flow or was engulfed by a tongue of the last flow at Site 1243. Unit 1 and Unit 3 have similar characteristics and are the same unit; the small piece of Unit 2 limestone should not have been considered a unit boundary. Therefore, there are six shipboard-identified units of basalt basement cored at the site. Shipboard petrography and ICP-AES geochemistry allowed shipboard petrologists to identify four units (1 plus 3, 5, 7, and 8) as tholeiitic and relatively unevolved and to characterize them as having had minimal differentiation at the crustal level. There was no shipboard ICP-AES analysis of Unit 6 (Table T6).

T6. ICP-AES analyses, p. 36.

Unit 4 is alkali basalt, based on shipboard petrography and geochemistry. Euhedral microphenocrysts of olivine in the groundmass and augite, as well as brown clinopyroxene, indicate alkaline affinities. By shipboard ICP-AES, K_2O of ~0.7 wt%, Na_2O of ~3.5 wt%, high Zr/Y and Ba/Sr, and low Ti/Zr are geochemical evidence of alkali basalt. Recovery of Unit 4 was relatively good; pieces totaling 8.97 m were recovered from the unit, which is ~14.8 m thick. Unit 4 is pillowed, sparsely to moderately vesicular, and only sparsely olivine- and plagioclase-phyric, indicating it was erupted on the seafloor and not emplaced as a sill at some unknown, later, post–rise crest time. There are no nearby seamounts that might be alkalic. Unit 4's present stratigraphic position in the upper oceanic crust, therefore, indicates that this alkaline unit was emplaced relatively late, but not last, at the spreading center.

Geochemical matches are few between shipboard ICP-AES analyses of units and microprobe analyses of glass cuttings. Three ICP-AES analyses of relatively thick Unit 3 are scattered (Fig. F11). Only Analysis 3-3, from Unit 3 at 130.1 mbsf (Fig. F1), lies within any of the glass groupings, and it plots in Group M. ICP-AES Analysis 8, from Unit 8 at 190.4 mbsf, lies within Group A. Not only do the other ICP-AES analyses lie outside the clustered SOEST analyses, they also do not lie along similar K_2O/TiO_2 ratios that might suggest a consanguineous link with the groupings.

F11. MgO vs. K_2O/TiO_2, p. 22.

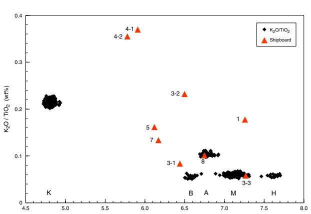

An argument might be made, however, that differences in analyses, as shown in Figure F11, result mainly from differences in material (whole-rock pillow interior vs. pillow margin glass) and instrument (ICP-AES vs. probe). If so, matches need not be overlaps but might be made between close-lying analyses. In that case, Unit 4 is closest to Group K on the basis of relatively low Mg and high alkalis. There are, however, problems matching Group K to Unit 4 when a plot of TiO_2 vs. Al_2O_3, CaO, and FeO is also considered (Fig. F12). Most significantly, Fe in Group K is higher than Ca and nearly approaches Al, whereas in the two ICP-AES analyses of Unit 4, Fe is lower than CaO and Al_2O_3 is especially high. Moreover, TiO_2 is distinctly higher in Group K than is shown in the Unit 4 analyses. If shipboard ICP-AES analyses of TiO_2, Al_2O_3, CaO, and FeO were the only basis for correlation, Group M might match Unit 3, whereas adjacent Groups A and H might be represented by Units 5 and 8, respectively. No group apparently matches Unit 7, with its high FeO content.

F12. TiO_2 vs. Al_2O_3, FeO, and CaO, p. 23.

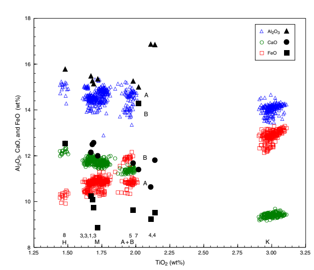

Thin sections probed at SOEST and ORI give additional geochemical information. The ORI raw microprobe data is of 27 samples that yielded 211 analyses. The set is concentrated on Units 3 (6 samples with 10 analyses each is 60 analyses) and 4 (13 samples with 10 analyses each is 130 analyses). The remaining few analyses are from deeper units (one sample of Unit 5 with five analyses, four samples of Unit 6 with one analysis each and one sample with five analyses, and two samples of Unit 8 with one analysis each and one sample with five analyses). As the ORI data are preliminary, without corrections or evaluations, we cannot place great weight on details. Nevertheless, some comments and conclusions are possible. The values for Units 3 and 4 plot in clusters on a graph of MgO vs. Al_2O_3, CaO, and FeO (Fig. F13). The five analyses of the Unit 5 sample fall within the cluster for Unit 3.

F13. Microprobe analyses, p. 24.

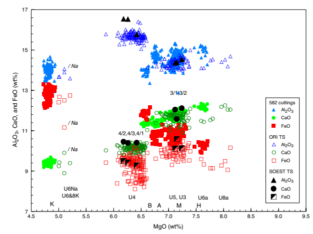

The ORI analyses of Unit 6, however, do not plot as a cluster but are distributed into three geochemical sets. Near the top of Unit 6, in Core 203-12443B-12R, the 160.70-mbsf sample has low MgO, moderately high TiO_2 and K_2O, and high Na_2O, and on Figure F13 it is termed "U6Na" and indicated by "/Na." Analysis U6Na is near three additional Unit 6 and one Unit 8 analyses with high K. That cluster, which is designated as "U6&8K," has the highest FeO and lowest MgO values of the ORI analyses. Next in depth for Unit 6 are three analyses of Core 203-12443B-13R (166.65, 166.97, and 167.02 mbsf) with relatively low MgO and CaO but high TiO_2, FeO, and K_2O values; these high-K analyses are in the arbitrary Group U6&8K. The five analyses of the Unit 6 sample from Core 203-12443B-14R at 172.13 mbsf are designated as "U6a" on Figure F13.

Shipboard Unit 7 was not analyzed on board the ship or at ORI. There was little recovery from Unit 8, but the ORI analyses of samples at 190.43 mbsf (five analyses) and 190.49 mbsf (one analysis), near the top of Unit 8, are designated as "U8a" on Figure F13. The deepest Unit 8 sample, from Core 203-1243B-18R at 190.67 mbsf, is high in Ti and K and plots with U6&8K. It should be noted that the pieces of core for Analyses U6a (Core 203-1243B-14R [Piece 27]; 172.13 mbsf) and eight of U6&8 (Core 203-1243B-18R [Piece 7]; 190.67 mbsf) are small and may have caved in and traveled down the hole to be recovered below their correct stratigraphic positions.

Microprobe analysis of thin sections at SOEST and ORI seem to raise as many new questions as they answer old ones about lava compositions and the source of the cuttings from the bottom of the hole. SOEST analyses of cuttings and thin sections are on the same instrument with the same procedures and remove possible concerns about comparing ICP-AES analyses with those from the probe, as discussed above. The succession of lavas at Site 1243 is considerably more complex than is indicated by the shipboard-defined units and their thicknesses, as given in the Leg 203 *Initial Reports* volume (Orcutt, Schultz, Davies, et al., 2003). Immediately apparent is that analyses of Units 3 and 5 plot together. Further, Analysis 3/2 of Unit 3 from Core 203-1243B-4R at ~121 mbsf plots with Unit 4. This is likely the result of a labeling problem on the ship during sampling or thin section preparation, as the depth is 20 m above the top of a gamma ray increase on the wireline log. It should be noted, however, that shipboard ICP-AES Analysis 3-2 of Unit 3 from Core 203-1243B-5R at ~124 mbsf has a moderately high K_2O (0.39 wt%).

Unit 4 lavas were not the source of Group K glass fragments (Fig. F13). Unit 4 has higher K_2O and Al_2O_3 and lower FeO content than

Group K and any other unit or group. Unit 4 also has a MgO content distinct from other units or groups (except Group B, which has different values of several other elements). Close to Group K, however, are U6&8K analyses, and perhaps sodium-rich 6Na belongs with U6&8K. Units 6 and 8 are from the part of the hole with poor recovery. SOEST and ORI analyses of Units 3 and 5 plot with Group M (Fig. **F11**), and the shipboard ICP-AES information also suggested that Unit 3 and Group M match (Fig. **F11**). The suggestion from ICP-AES that Unit 5 matches Group A is equivocal with the microprobe information; Al_2O_3, CaO, and FeO values agree, but MgO in the thin sections is ~0.3 wt% higher. Group H is close to U6a.

Relationships between SOEST and ORI analyses are extended to a wider range of elements. SOEST Group K and ORI Analyses U6&8K resemble each other not only in MgO, Al_2O_3, FeO, and CaO (Fig. **F13**) but also in K_2O (Fig. **F14**). Analyses U6a is intermediate between Groups M and H, except that it is low in SiO_2. If indeed ORI silica values were increased by ~1 wt%, or SOEST values decreased by that amount, differences between ORI and SOEST analyses nearly disappear.

F14. Thin section analyses, p. 25.

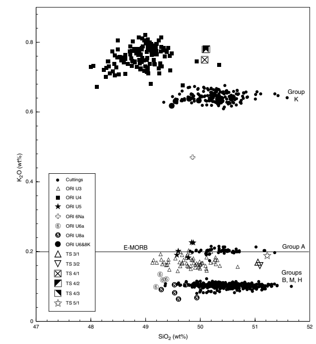

Enriched Mid-Ocean-Ridge Basalt and a Possible Galápagos Source

Glasses from the Galápagos region (Cushman et al., 2004) were used to define E-MORB as having >0.2 wt% K_2O and >0.15 K/Ti (Figs. **F14, F15**). Leg 203 rocks and glasses give mixed results using these classifications. Although Unit 4 samples plot within the E-MORB field on both diagrams, Group K plots in the E-MORB field for K_2O but not for K/Ti. The Group A/Unit 5 samples have similar features. These features suggest that the Ti content for the source of the Leg 203 basalts is higher than for the Galápagos MORB.

F15. MgO vs. K/Ti, p. 26.

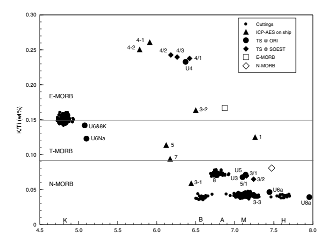

MORB near presumed mantle plumes commonly has a compositional gradient in incompatible minor and trace elements and heavy rare earth elements (e.g., Schilling, 1973; le Roux et al., 2002, and references therein). Ocean crust of the Galápagos region is well known for its enriched basalts (McBirney, 1993; Cushman et al., 2004, and references therein). At the Galápagos triple junction, the Pacific-Cocos part of the East Pacific Rise is spreading at ~137 mm/yr, and the Cocos-Nazca Ridge, or Galápagos spreading center, is spreading at ~41 mm/yr, while the triple junction propagates westward at ~66 mm/yr. The Galápagos gore, a crude triangle of irregular topography pointing west toward the triple junction, is oceanic crust that formed on the Cocos-Nazca Ridge (Fig. **F16**). In the present day, the Galápagos spreading center has three well-defined provinces that differ in geochemistry, geophysics, and bathymetry (Detrick et al., 2002). From the triple junction eastward to 95.5°W, a ridge of relatively low topography is composed of N-MORB. The middle province, of intermediate topography and geochemistry, is bounded on the west by the tip of a propagating rift at 95.5°W and on the east by an increase in topography and basalt enrichment at 92.6°W. The relatively high ridge crest between 92.6°W and 90.5°W is composed of E-MORB (Cushman et al., 2004). This segment and the adjacent Galápagos Islands mark the Galápagos hotspot or assumed plume.

F16. Site 1243, p. 27.

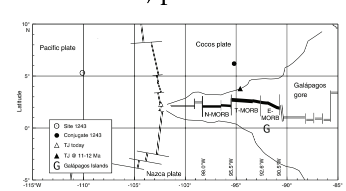

Site 1243 is located on the Pacific plate between the triple junction and Siqueiros Fracture Zone, ~900 km west of the rise crest. If the site is restored to its rise-crest position at ~11 or 12 Ma, the conjugate point on the Cocos plate would today be at ~6°10′N, 95°20′W. At that time of crustal generation, the Galápagos spreading center would have been ~2.5° or ~280 km south of the site (Fig. **F16**). The middle province, of transitional (T)-MORB, is today the rise-crest province closest to the conjugate point for Site 1243. Unit 4 basalt at Site 1243, however, plots within the analyses of the E-MORB province that is now on the rise-crest east of 92.6° and Group K plots on the boundary between E-MORB and T-MORB composition, as determined by Cushman et al. (2004). Figure **F16** and this discussion are simply intended to show that ocean crust at Site 1243 formed near a presumed enriched mantle plume. Because the history of rifting and island formation relative to an enriched mantle source have been complex, one cannot conclude that a specific MORB-type segment of today's ridge crest predominated during formation of the basalts recovered from Site 1243.

Whereas the Galápagos spreading center today has clear geochemical segmentation, the East Pacific Rise north of the triple junction at 11–12 Ma had two distinct geochemical sources of magma, one normal and one enriched, that fed Site 1243 lavas. Thus it is possible that enriched basalts from Site 1243 represent a signature of the Galápagos hotspot in the crust of the Pacific plate. The alternative, however, is that both N-MORB and E-MORB can be erupted close in space and time, depending on such factors as mantle enrichment, mantle thermal regime, and spreading rate. E-MORB, along with N-MORB, is known at the ridge crest as far north as the Juan de Fuca Ridge (Karsten et al., 1990) and as far south as the southern Chile Ridge (Sherman et al., 1997). Although composition varies along the ridge crest and is generally segmented between transforms, these localities show source heterogeneity. Bergmanis et al. (2004) used submersible observations and isotopic and other geochemical data, including concentrations of incompatible elements, to show that seven compositionally distinct lava types from two chemically distinct parental magmas erupted on a 24-km-long segment of the East Pacific Rise at 17°S within several hundred years. Therefore, a drilled section in one of these areas is likely to penetrate a random succession of N-MORB and E-MORB.

SUMMARY

Comparison of microprobe work on glass cuttings and thin sections with the shipboard ICP-AES and ORI microprobe work has shown the following:

1. The cuttings came mostly, if not entirely, from the lower part of Hole 1243B because geochemically distinct Units 3 and 4 of the upper part of the hole are not present in the analyzed cuttings. Distinctive, alkalic Unit 4 is represented by several cores from high in the drilled basement section but it is not represented by even one of the 582 cuttings analyzed from the bottom of the hole. Tholeiitic Units 1, 3, and 5, from the upper to middle part of the section, resemble each other, but although Group M is similar to those units in MgO and CaO content, its lower SiO_2, Al_2O_3, and FeO indicate that Group M, representing more than one-half of the cuttings, is not from a Unit 1, 3, or 5 source.
2. Group K is close to Analyses U6&8K and fairly close to Analysis U6Na in nearly all components (SiO_2, TiO_2, K_2O, Al_2O_3, CaO, FeO, and MgO). Therefore, Group K probably came from ~160

mbsf and deeper and may extend as deep as Section 203-1243R-18R-1 (Piece 7) at 190.67 mbsf (the “8” in U6&8K), a piece so small it may have caved and fallen from that higher level. The substantial fraction of Group K in the cuttings, in spite of the intensive effort to sweep the hole clean and the thick section of cavings, wide caliper readings, and lower sonic velocities, indicates that a significant part of the lower part of Site 1243 is of Group K composition.

3. Group M, because of its abundance, probably came from below 170 mbsf, deep in the hole where recovery was especially poor and analyses are few.
4. Group A probably matches Unit 5, which was sampled at ~156 mbsf.
5. Nothing plots close to Group B, and it may be a slight differentiate of Group M.
6. Group H may match Unit 6 near 167 mbsf or perhaps Unit 8 at 190 mbsf if only a few elements or ratios are considered. Group H may also be a slight differentiate of Group M.
7. Considering the total evidence of the cores, the cuttings and their likely depths of source, the numbers of analyses, the gamma ray log for Unit 4, and the apparent cavings history for Group K, approximately two-thirds of the penetrated basement is N-MORB and one-third (Unit 4, Group K, and perhaps Unit 5/Group A) is enriched or T-MORB.
8. The combination of normal and enriched basalts, indicating two distinct parental magmas, may be a record of the Galápagos plume, or it may be a consequence of spreading rate and mantle thermal regime.

ACKNOWLEDGMENTS

This research used samples and data provided by the Ocean Drilling Program (ODP). ODP is sponsored by the National Science Foundation (NSF) and participating countries under management of Joint Oceanographic Institutions (JOI), Inc. Funding for this research was provided by NSF through the Texas A&M Research Foundation (TAMURF). John Sinton gave a number of helpful comments. This is SOEST Contribution 6751.

REFERENCES

Bergmanis, E.C., Sinton, J.M., Rubin, K.H., Mahoney, J.J., Bowles, J., Gee, J.S., and Smith, M.C., 2004. Magma reservoir dynamics and diverse mantle melting at the southern East Pacific Rise: 17°22′S–17°35′S. *Eos, Trans. Am. Geophys. Union,* 85(47):V53A-0611. (Abstract)

Cushman, B., Sinton, J.M., Ito, G., and Dixon, J.E., 2004. Glass compositions, plume-ridge interaction, and hydrous melting along the Galápagos spreading center, 90.5°W to 98°W. *Geochem., Geophys., Geosyst.,* 5:Q08E17. **doi:10.1029/2004GC000709**

Detrick, R.S., Sinton, J.M., Ito, G., Canales, J.P., Behn, M., Blacic, T., Cushman, B., Dixon, J.E., Graham, D.W., and Mahoney, J.J., 2002. Correlated geophysical, geochemical, and volcanological manifestations of plume-ridge interaction along the Galápagos spreading center. *Geochem., Geophys., Geosys.,* 3. **doi:10.1029/2002GC000350**

Karsten, J.L., Delaney, J.R., Rhodes, J.M., and Liias, A., 1990. Spatial and temporal evolution of magmatic systems beneath the Endeavour segment, Juan de Fuca Ridge: tectonic and petrologic constraints. *J. Geophys. Res.,* 95:19235–19256.

le Roux, P.J., le Roex, A.P., Schilling, J.-G., Shimizu, N., Perkins, W.W., and Pearce, N.J.G., 2002. Mantle heterogeneity beneath the southern Mid-Atlantic Ridge: trace-element evidence for contamination of ambient asthenospheric mantle. *Earth Plant. Sci. Lett.,* 203:479–498. **doi:10.1016/S0012-821X(02)00832-4**

Macdonald, G.A., and Katsura, T., 1964. Chemical composition of Hawaiian lavas. *J. Petrol.,* 5:82–133.

McBirney, A.R., 1993. *Igneous Petrology* (2nd. ed.): Boston (Jones and Bartlett).

Orcutt, J.A., Schultz, A., Davies, T.A., et al., 2003. *Proc. ODP, Init. Repts.,* 203 [CD-ROM]. Available from: Ocean Drilling Program, Texas A&M University, College Station TX 77845-9547, USA. [**HTML**]

Schilling, J.-G., 1973. Iceland mantle plume: geochemical study of Reykjanes Ridge. *Nature (London, U. K.),* 242:565–571. **doi:10.1038/242565a0**

Sherman, S.B., Karsten, J.L., and Klein, E.M., 1997. Petrogenesis of axial lavas from the southern Chile Ridge: major element constraints. *J. Geophys. Res.,* 102:14963–14990. **doi:10.1029/97JB00510**

Shipboard Scientific Party, 2003a. Leg 203 summary. *In* Orcutt, J.A., Schultz, A., Davies, T.A., et al., *Proc. ODP, Init. Repts.,* 203: College Station TX (Ocean Drilling Program), 1–30. [**HTML**]

Shipboard Scientific Party, 2003b. Site 1243. *In* Orcutt, J.A., Schultz, A., Davies, T.A., et al., *Proc. ODP, Init. Repts.,* 203, 1–85 [CD-ROM]. Available from: Ocean Drilling Program, Texas A&M University, College Station TX 77845-9547, USA. [**HTML**]

Figure F1. Basement section in Hole 1243B with locations of lithologic units, cores, and analyses. Basement Units 1 and 3 are the same lithology, separated in the recovered core by a 2-cm piece of limestone that was designated as Unit 2. Core 203-1243B-19R provided the 582 glass cuttings discussed in this report. Inductively coupled plasma–atomic emission spectroscopy (ICP-AES) analyses made on board are given in the format "unit number-analysis number" (e.g., Analysis 3-1 is the first analysis of Unit 3). Thin-section analyses (TS) performed at Ocean Research Institute (ORI), University of Tokyo (UT), are designated by the letter U (for unit) and a number. Thin-section analyses at School of Ocean and Earth Sciences and Technology (SOEST), University of Hawaii (UH) are given in the format "unit number/analysis number" (e.g., Analysis 3/1 is the first analysis of Unit 3).

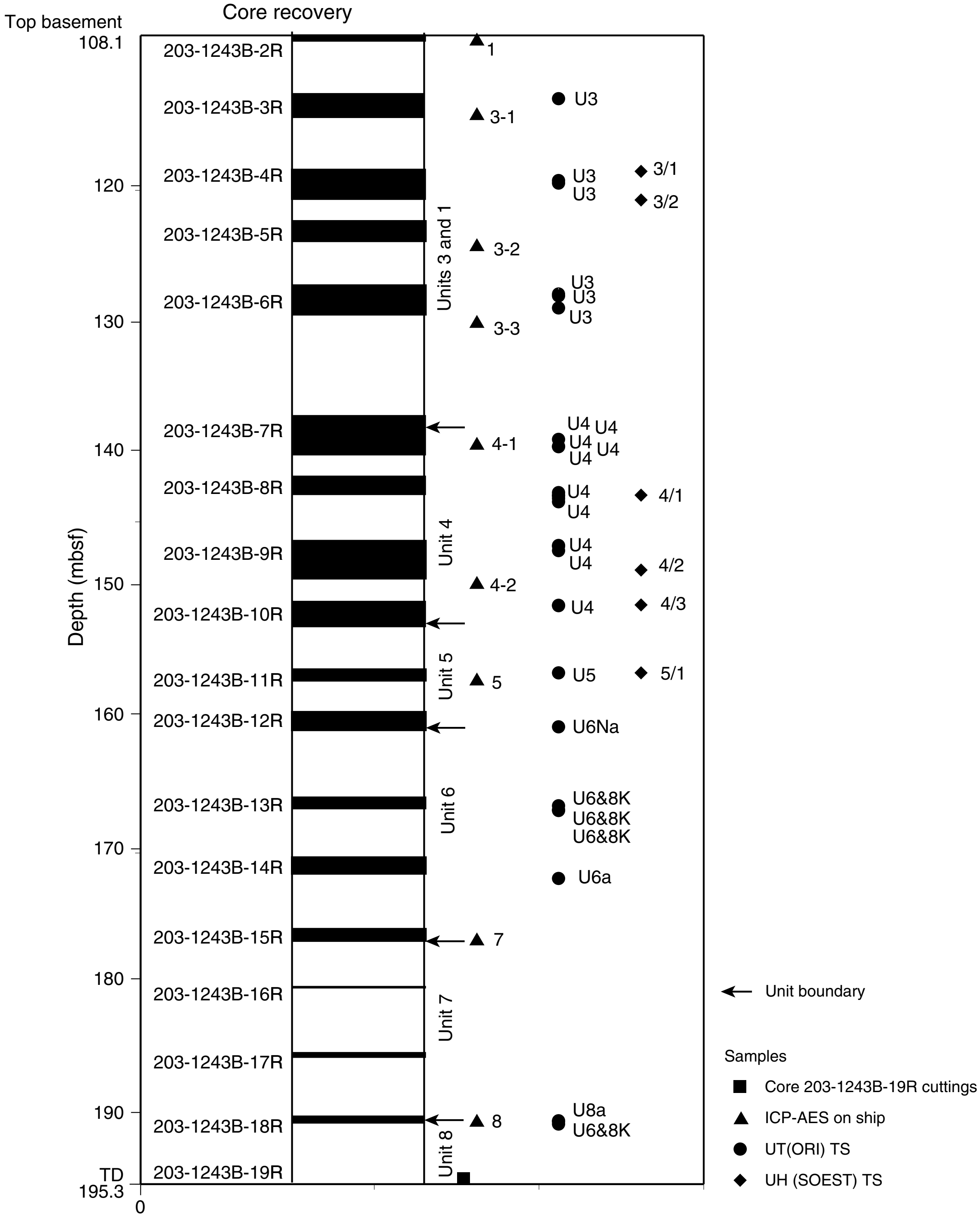

Figure F2. MgO vs. K_2O/TiO_2 electron microprobe analyses performed at University of Hawaii. Two of the points are averages (arithmetic mean) of three electron microprobe analyses per sample. The remaining 580 points are averages of four analyses per sample. Analyses clustered into five groups. Group designations and numbers of analyses per group (in parentheses) are listed.

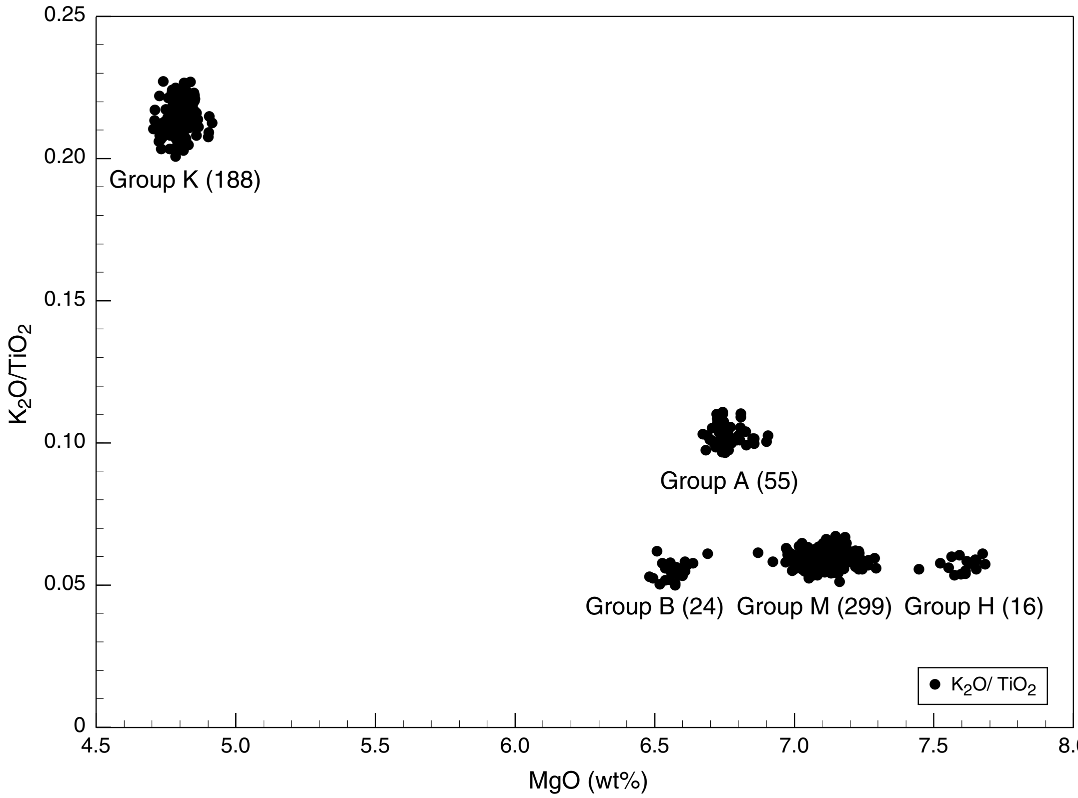

Figure F3. Silica vs. total alkalies. Dashed line separates Hawaiian lavas of alkalic mineral composition from Hawaiian lavas of tholeiitic mineral composition (Macdonald and Katsura, 1964). Diamond = normal mid-ocean-ridge basalt as average basaltic glass from Atlantic, Pacific, and Indian Ocean spreading centers, square = enriched mid-ocean-ridge basalt as average basalt from vicinity of Galapagos hotspot on the Galapagos spreading axis (from table 8-1 in McBirney, 1993).

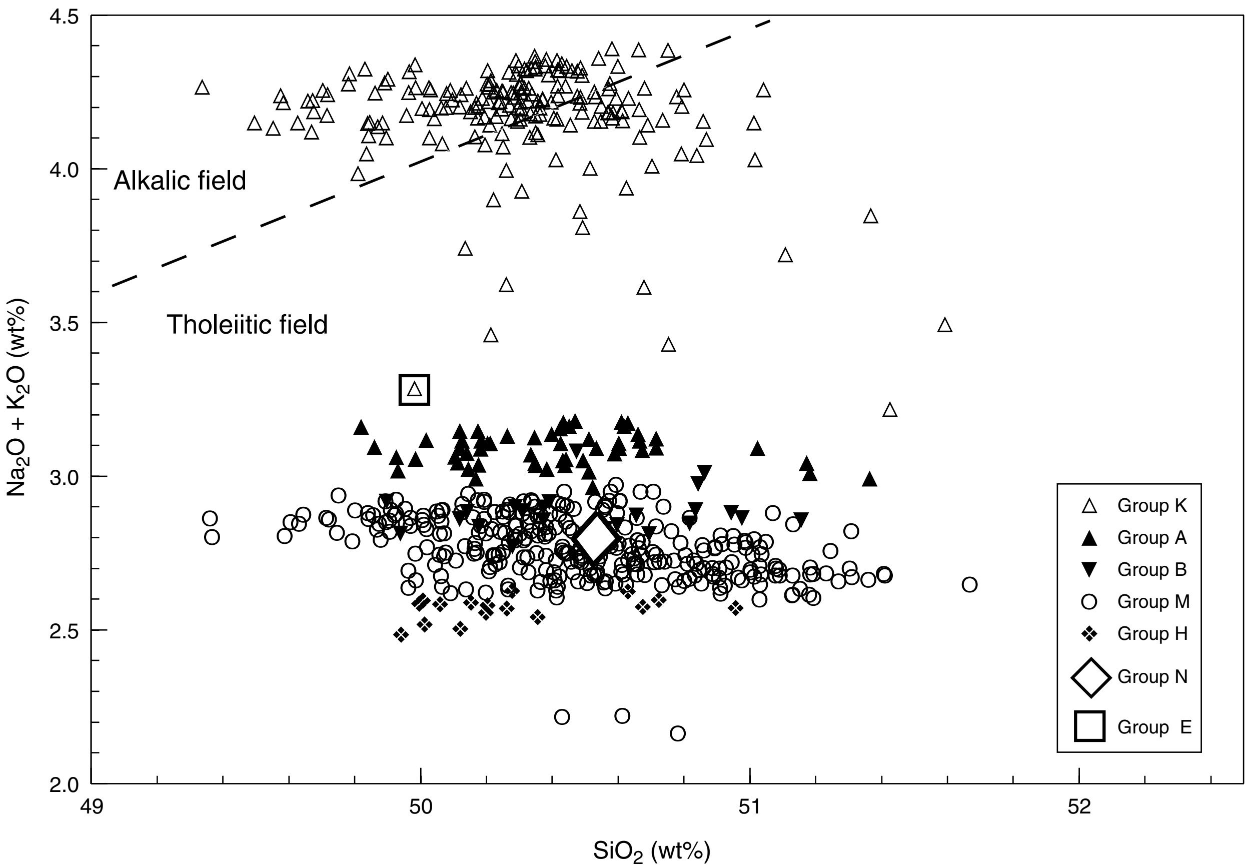

Figure F4. SiO_2 vs. K_2O. The line at 0.2 wt% K_2O is a lower boundary of enriched mid-ocean-ridge basalt (E-MORB) (Cushman et al., 2004). Open diamond = normal mid-ocean-ridge basalt as average basaltic glass from Atlantic, Pacific, and Indian Ocean spreading centers, open square = E-MORB as average basalt from vicinity of Galapagos hotspot on the Galapagos spreading axis (from table 8-1 in McBirney, 1993).

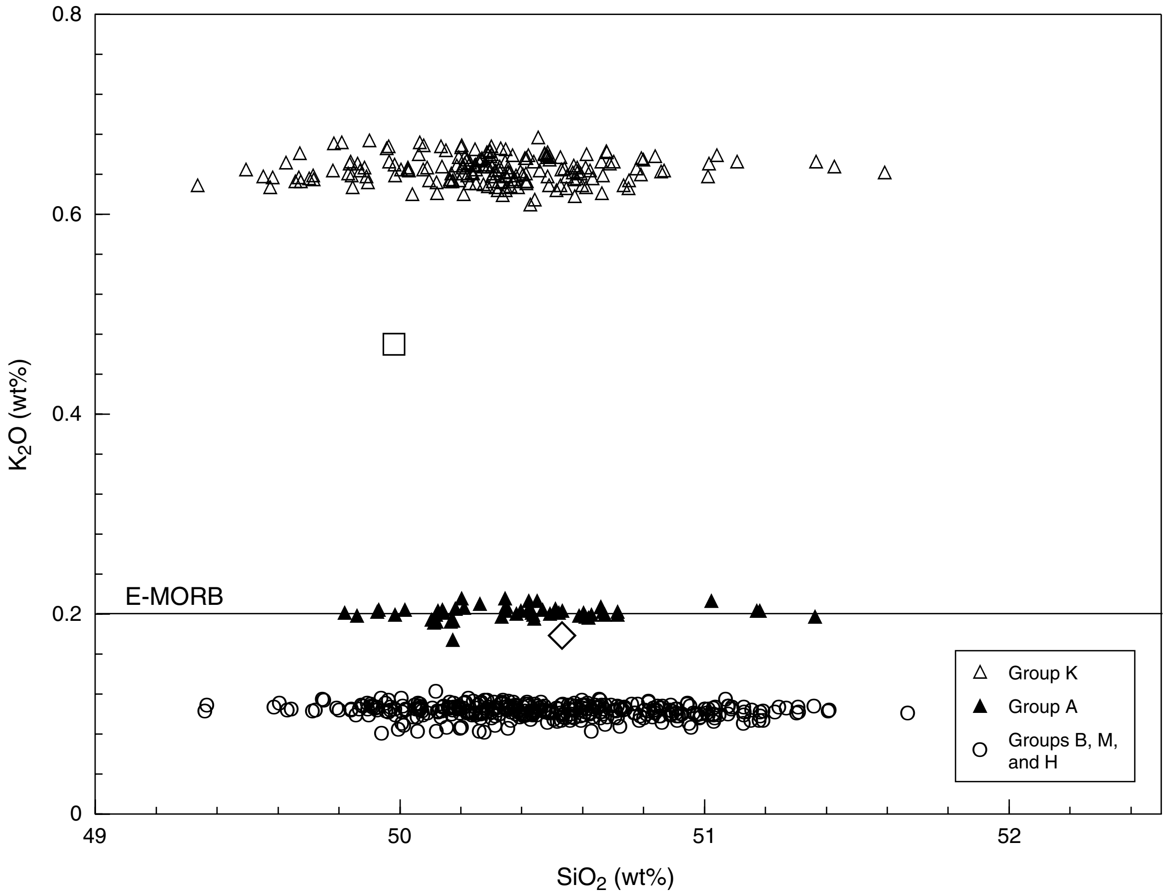

Figure F5. MgO vs. Al_2O_3, CaO, and FeO. Groups are identified by letters along the bottom of the graph. Note gap in values between 5 and 6.5 wt% MgO. Averages of E-MORB at ~6.8% MgO and N-MORB at ~7.5% MgO indicated by large open symbols.

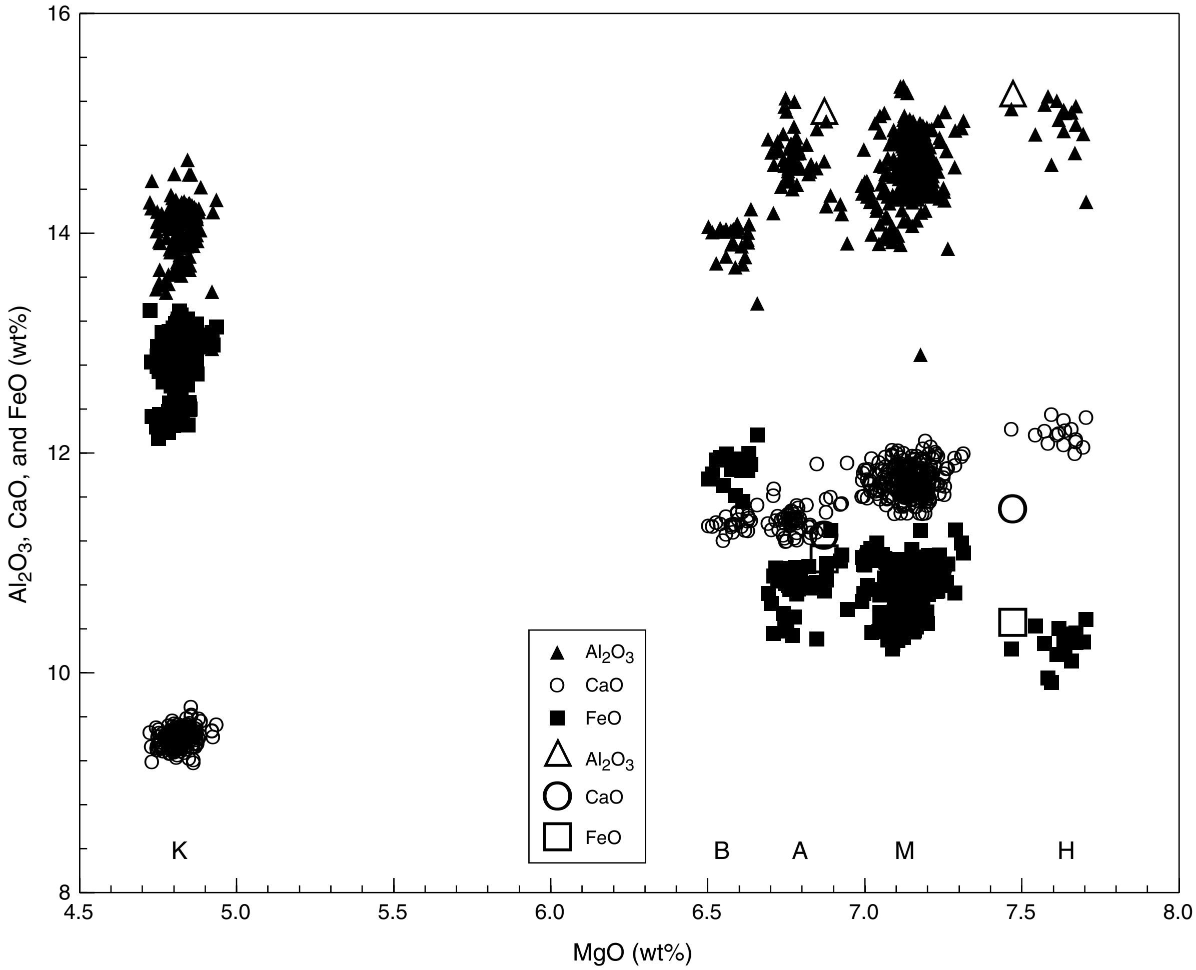

Figure F6. Detail of MgO vs. Al_2O_3, CaO, and FeO for Groups B, A, M, and H from Figure F5, p. 16. Groups are identified by letters along the bottom of the graph.

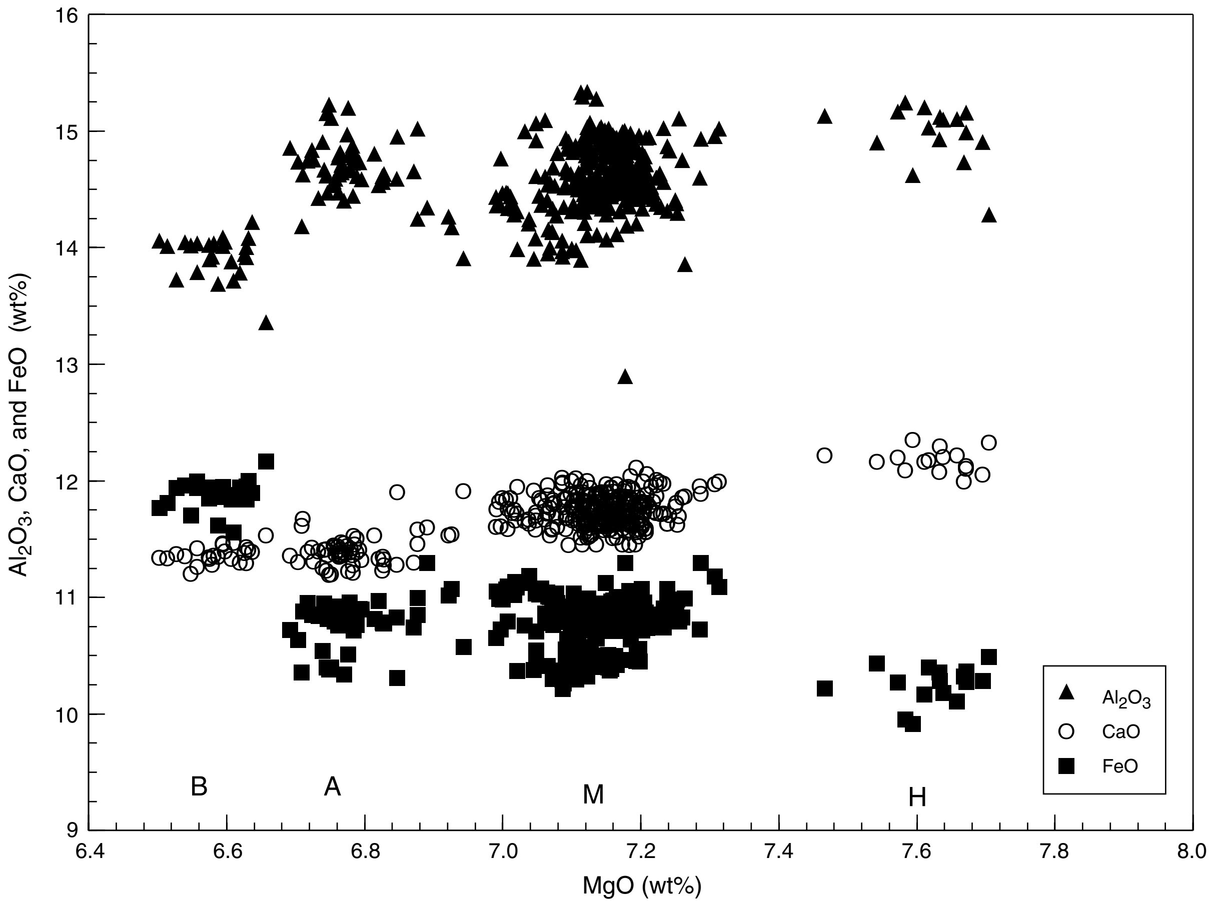

Figure F7. TiO_2 vs. Al_2O_3, CaO, FeO, and MgO. Groups are identified by letters along the bottom of the graph. Note Group A has less Al_2O_3 and more FeO than Group B. Averages of N-MORB at ~1.56% TiO_2 and E-MORB at ~1.99% TiO_2 are indicated by large open symbols.

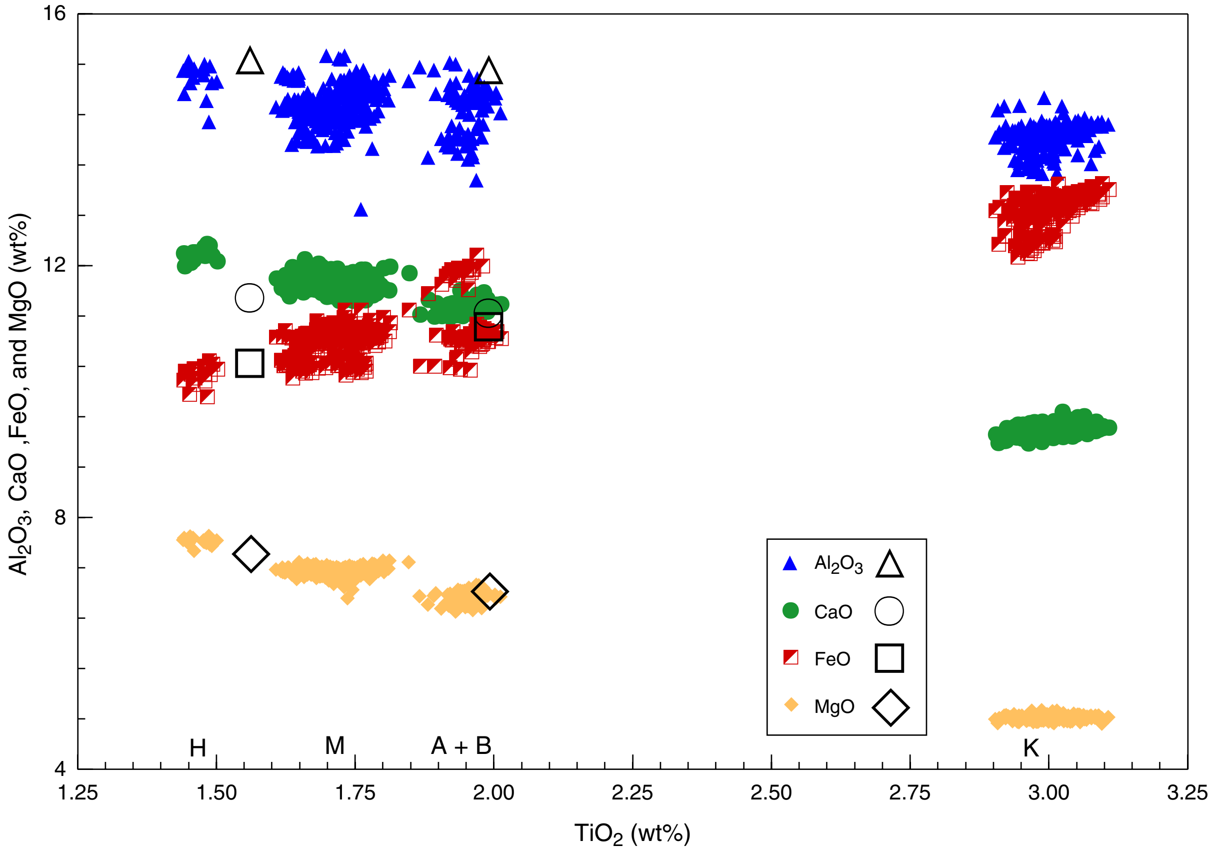

Figure F8. Detail of TiO_2 vs. Al_2O_3, CaO, FeO, and MgO for Groups A and B from Figure F7, p. 18.

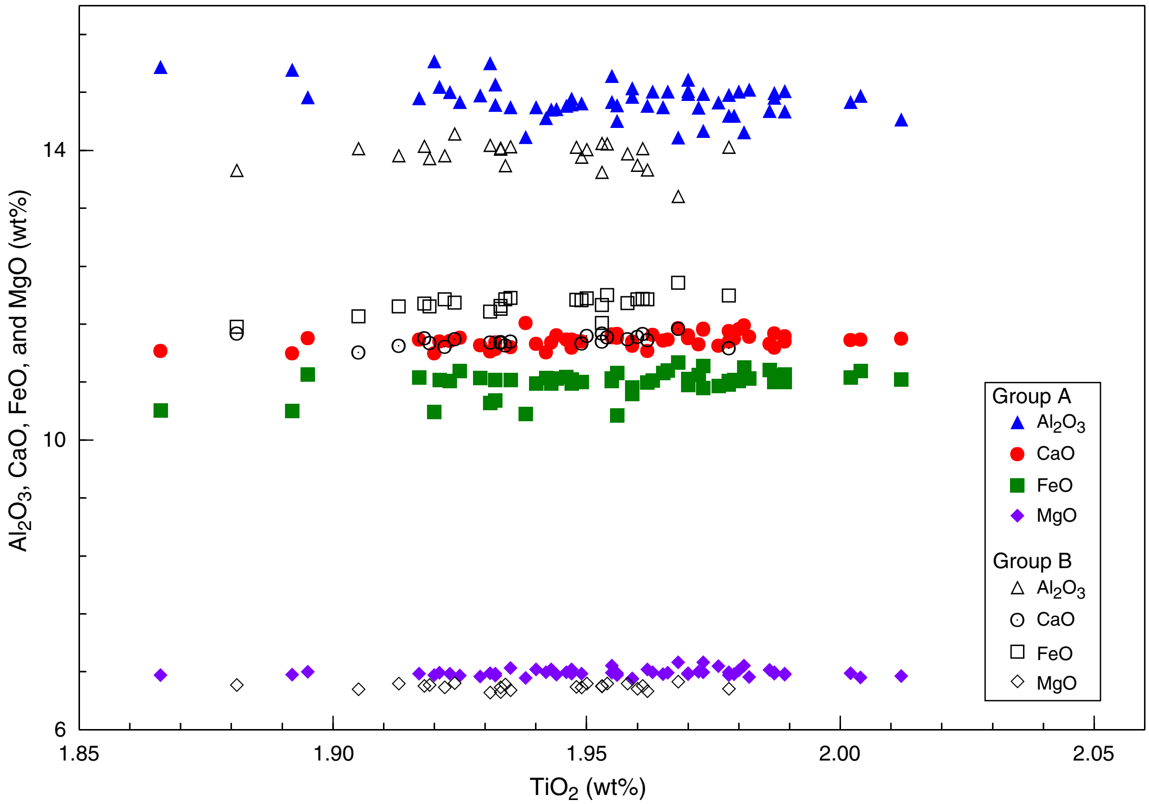

Figure F9. FeO vs. S, K_2O, and P_2O_5 for Groups M and K. Groups are identified by letters along the bottom of the graph the number of samples in parentheses. Minima in FeO analyses are at ~10.6 wt% in Group M and ~12.5 wt% in Group K.

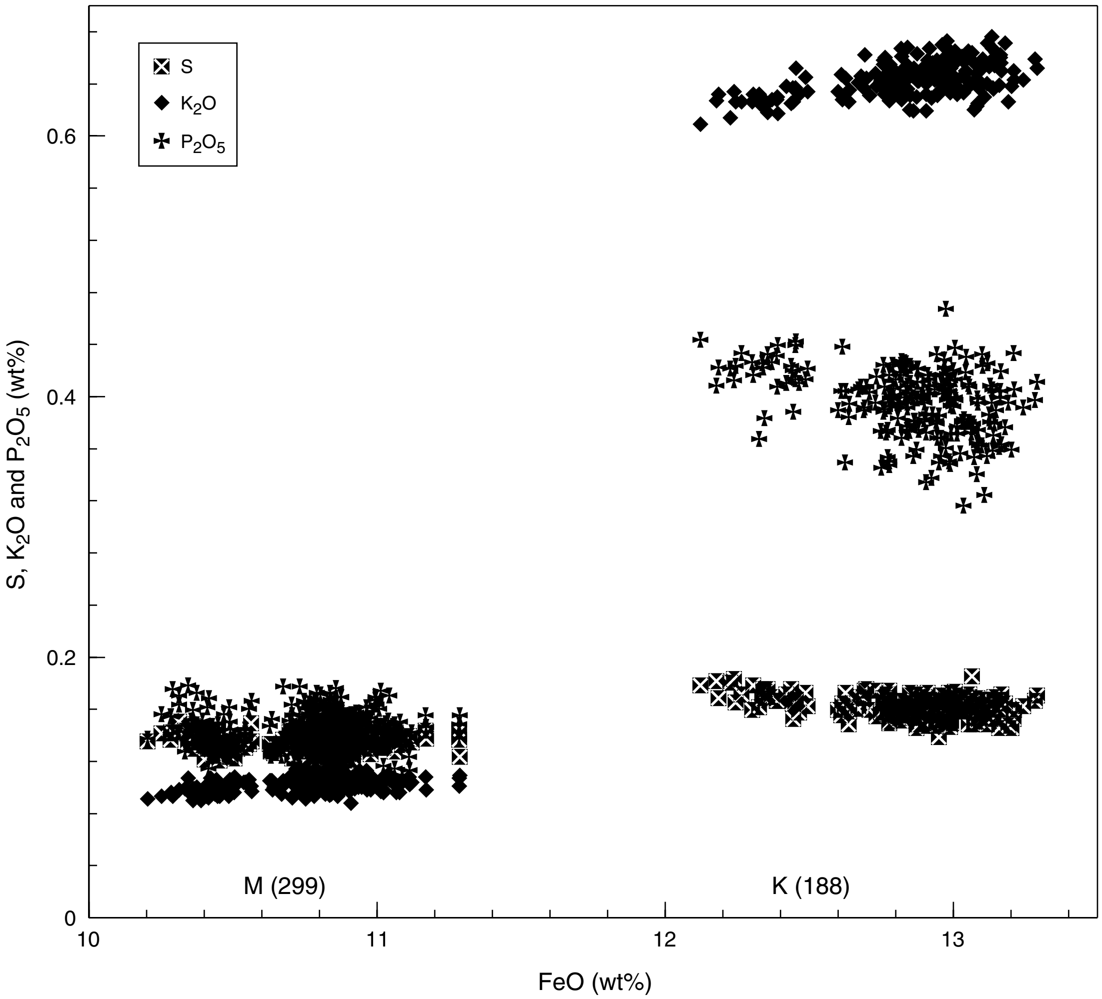

Figure F10. FeO vs. Al_2O_3, CaO, and MgO for Groups M and K in a semi-log plot to accommodate the range of values.

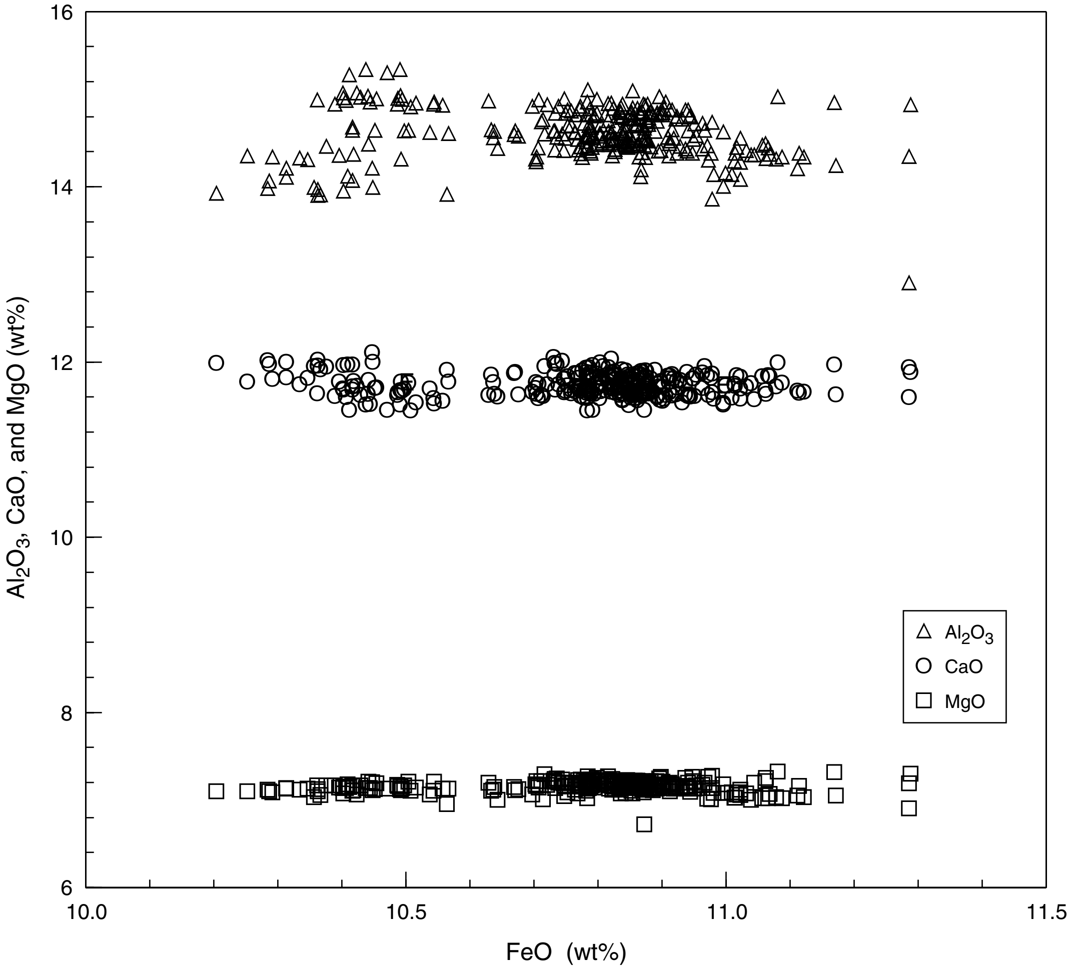

Figure F11. MgO vs. K_2O/TiO_2. Solid triangles indicate the nine shipboard ICP-AES analyses of pillow interiors, presumably nonglassy, of units identified on board. 1 = Unit 1 analysis; 3-1 = Unit 3, analysis 1; 3-2 = Unit 3, analysis 2; 3-3 = Unit 3, analysis 3; 4-1 = Unit 4, analysis 1; 4-2 = Unit 4, analysis 2; 5 = Unit 5; 7 = Unit 7; 8 = Unit 8. Note that geochemical correlation is poor, with matches only between Group A and Unit 8, and Group M and one analysis of Unit 3.

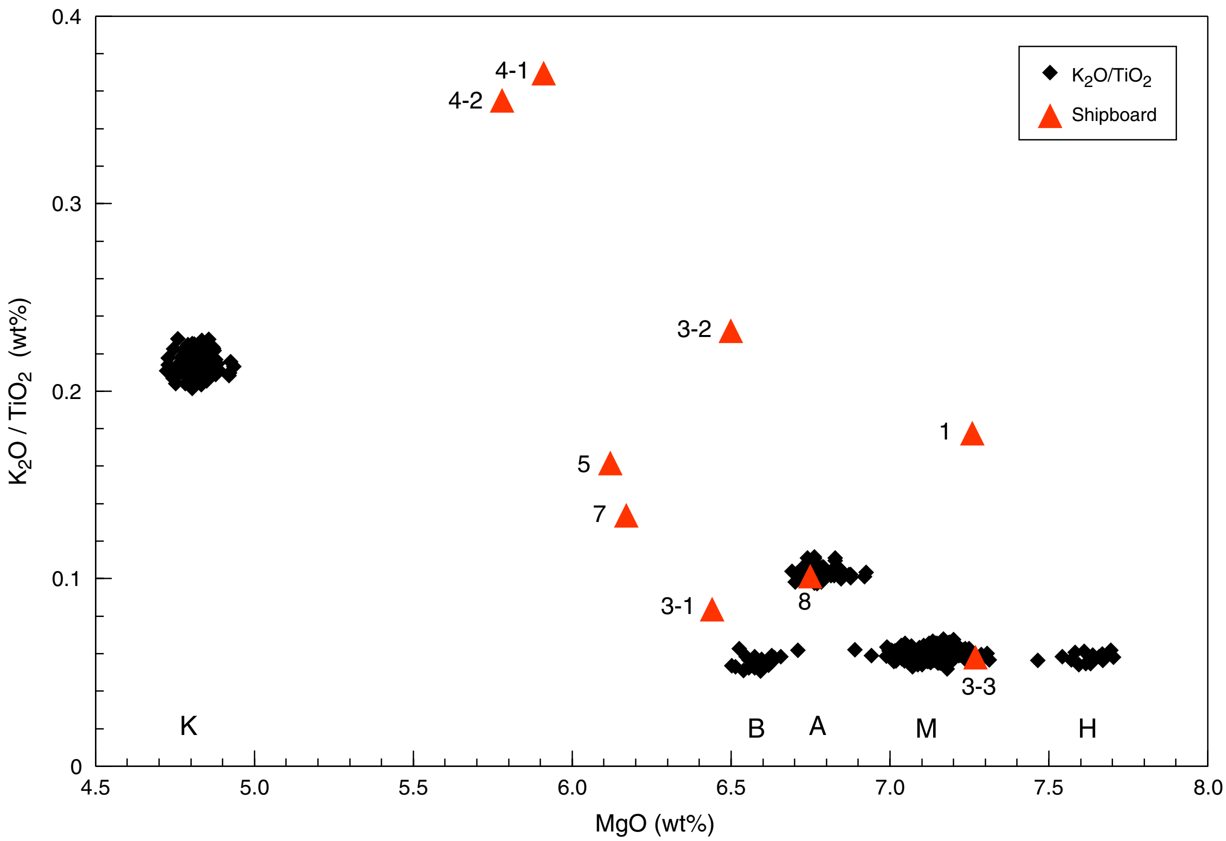

Figure F12. TiO_2 vs. Al_2O_3, FeO, and CaO. See also Figure **F7**, p. 18. Groups are identified by letters along the bottom of the graph. Groups A and B for Al and Fe are also identified within the graph (for Al, Group A > Group B; for Fe, Group B > Group A; for Ca, Group A = Group B). Solid symbols indicate the three oxides in the shipboard ICP-AES analyses of identified units. The numbers above the group letters along the bottom of the graph represent, left to right, one analysis of Unit 8, three analyses of Unit 3 with one analysis of Unit 1, one analysis of Unit 7, and two analyses of Unit 4.

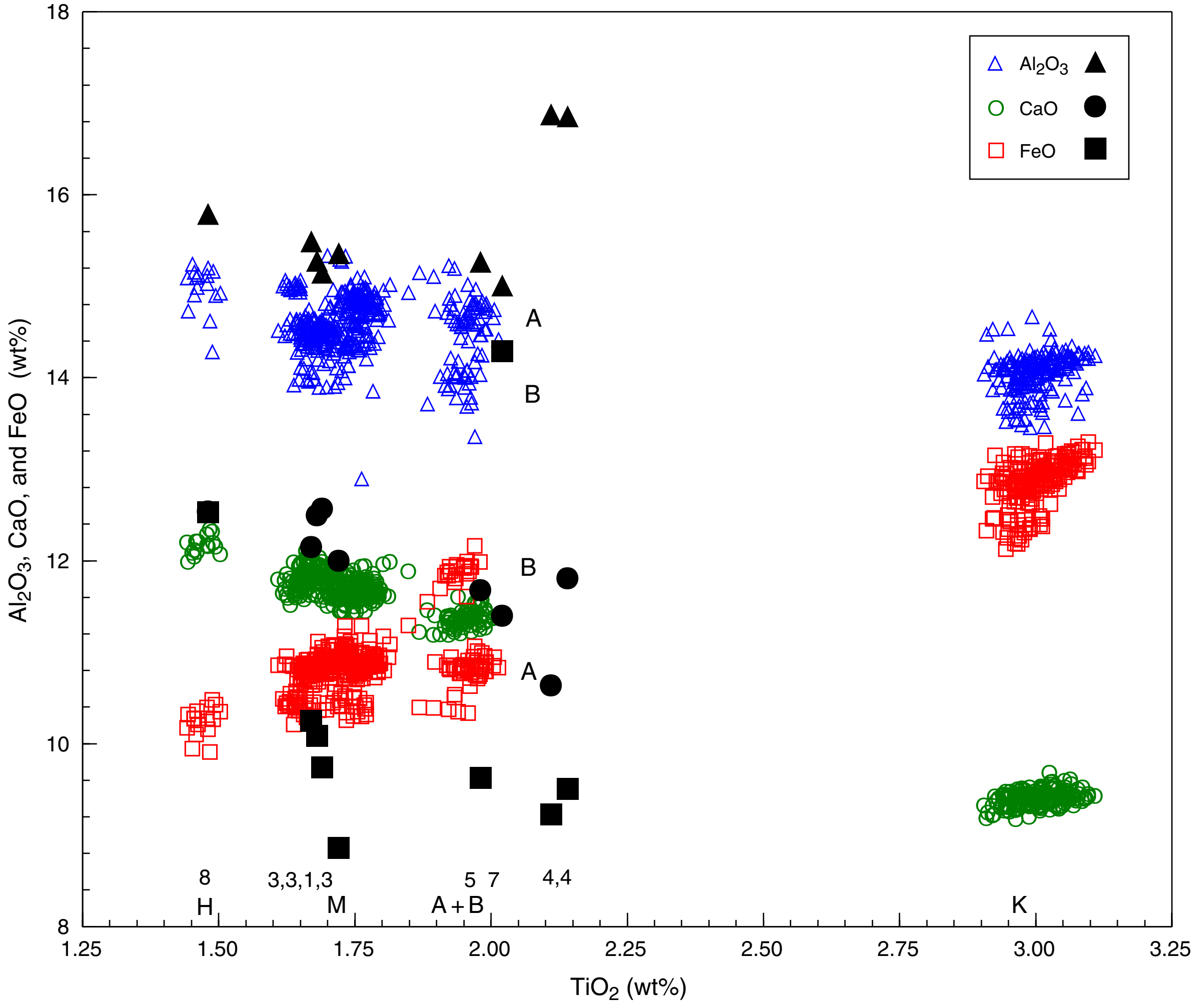

Figure F13. MgO vs. Al_2O_3, CaO, and FeO from microprobe analyses comparing glass cuttings and glass in thin sections of known stratigraphic position. Groups are identified by letters along the bottom of the graph. Small solid symbols = School of Ocean and Earth Sciences and Technology (SOEST) analyses of 582 cuttings, open symbols = raw unaveraged analyses of 28 thin section (TS) samples from shipboard-identified units, Ocean Research Institute (ORI), University of Tokyo. Groups of ORI analyses are identified along the bottom of the graph: U3 = 60 analyses of Unit 3; U4 = 130 analyses of Unit 4; U5 = five analyses of Unit 5; U6Na = one analysis of Unit 6 with high Na; */Na* = three geochemical sets within the U6Na analyses; U6a = five analyses of Unit 6 with low Na and K; U8a = six analyses of Unit 8 with low Na and K; U6&8K = four analyses of Unit 6 and one of Unit 8 with high K and low Mg (see text). Large solid symbols = averaged analyses of glass in six thin sections from shipboard-identified units analyzed at SOEST. Thin-section analyses are identified as follows: 3/1 and 3/2 = two analyses from Unit 3; 4/2, 4/3, and 4/1 = three analyses from Unit 4; and 5/1= one analysis from Unit 5.

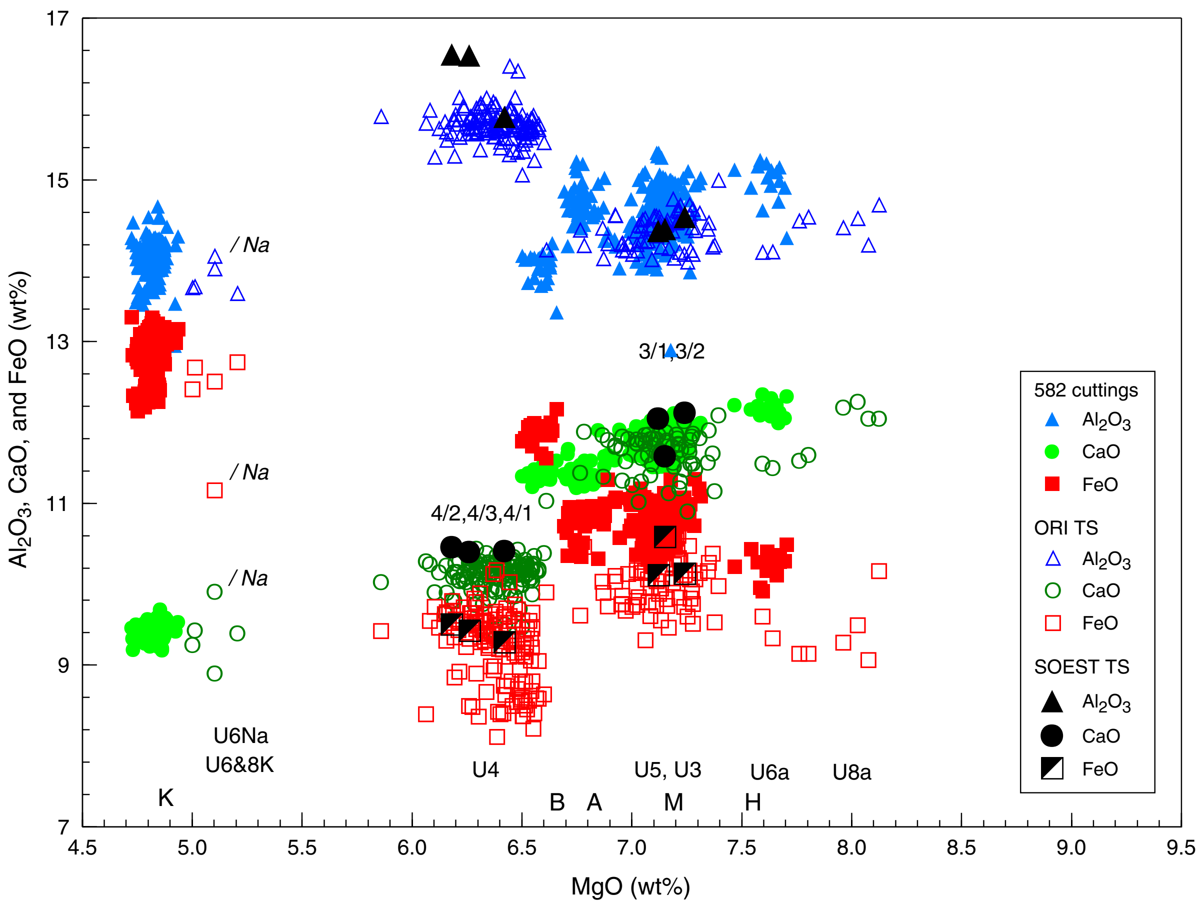

Figure F14. SiO_2 vs. K_2O. See also Figure F4, p. 15. Analyses of thin section (TS) glass at Ocean Research Institute (ORI) and SOEST are identified by units as in Figure F13, p. 24. E-MORB = enriched mid-ocean-ridge basalt.

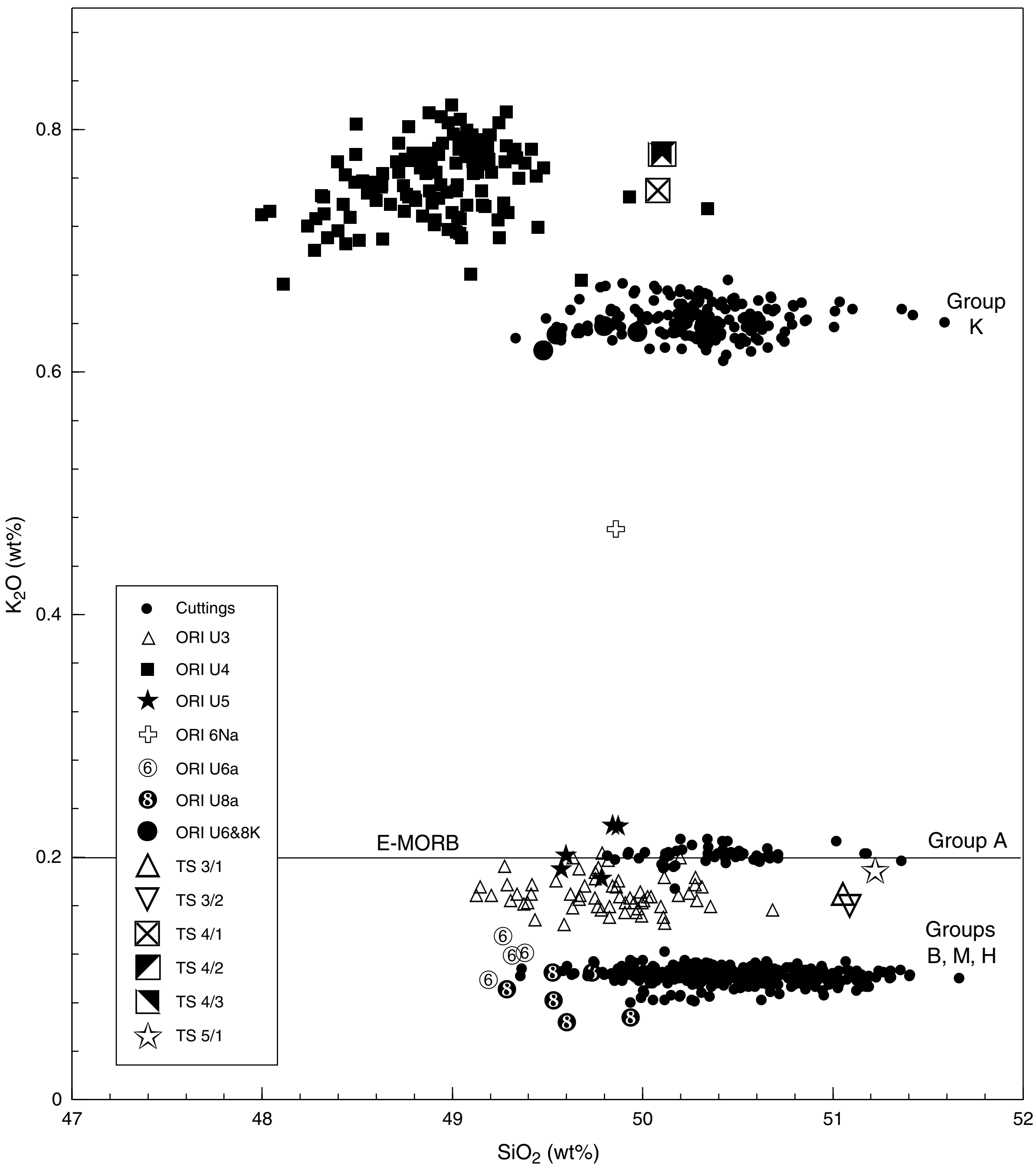

Figure F15. MgO vs. K/Ti as related to mid-ocean-ridge basalt (MORB) types. Microprobe analyses at School of Ocean and Earth Sciences and Technology (SOEST) of 582 cuttings are in groups labeled K, A, B, M, and H along the bottom of the graph. Solid triangles indicate the nine shipboard inductively coupled plasma–atomic emission spectroscopy (ICP-AES) whole-rock analyses of rock units identified on board (labeled as in Figure **F11,** p. 22). Solid circles are arithmetic means of Ocean Research Institute (ORI) raw microprobe analyses (labeled as in Figure **F13,** p. 24). Solid diamonds are SOEST microprobe analyses of glass in thin sections (TS) of five samples from three shipboard units (labeled as in Figure **F13,** p. 24). Transitional-type MORB (T-MORB) identified by Cushman et al. (2004) along the Galápagos spreading center lies mainly between K/Ti ratios of 0.09 and 0.15. Open symbols are averages for normal-type (N-MORB) and enriched-type (E-MORB), according to McBirney (1993).

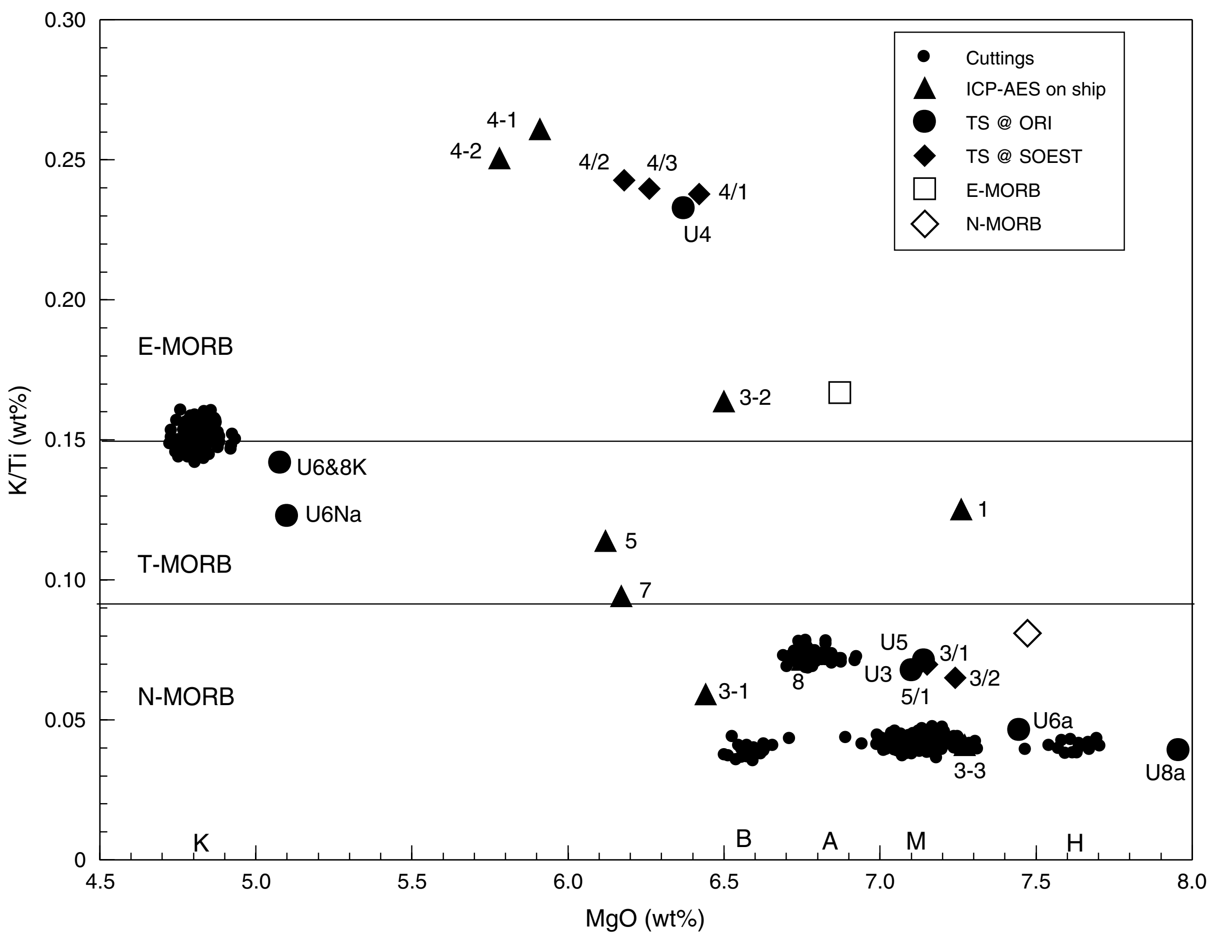

Figure F16. A portion of the eastern equatorial Pacific with Site 1243 and the Galápagos region. Site 1243, shown on the Pacific plate, has its conjugate point shown on the Cocos plate. Galápagos gore is the area of rough topography formed by the slower-spreading Galápagos Ridge. The Galápagos triple junction (TJ) at the time of crustal formation at Site 1243 is shown at the north edge of the gore. Topographic and geochemical segments today along the Galápagos spreading center are from Detrick et al. (2002) and Cushman et al. (2004). The Galápagos Islands and the transitional-type mid-ocean-ridge basalt (T-MORB) and enriched-type mid-ocean-ridge basalt (E-MORB) segments of the ridgecrest are manifestations of a presumed mantle plume, and basalt geochemistry at Site 1243 may have been affected by the plume. N-MORB = normal mid-ocean-ridge basalt.

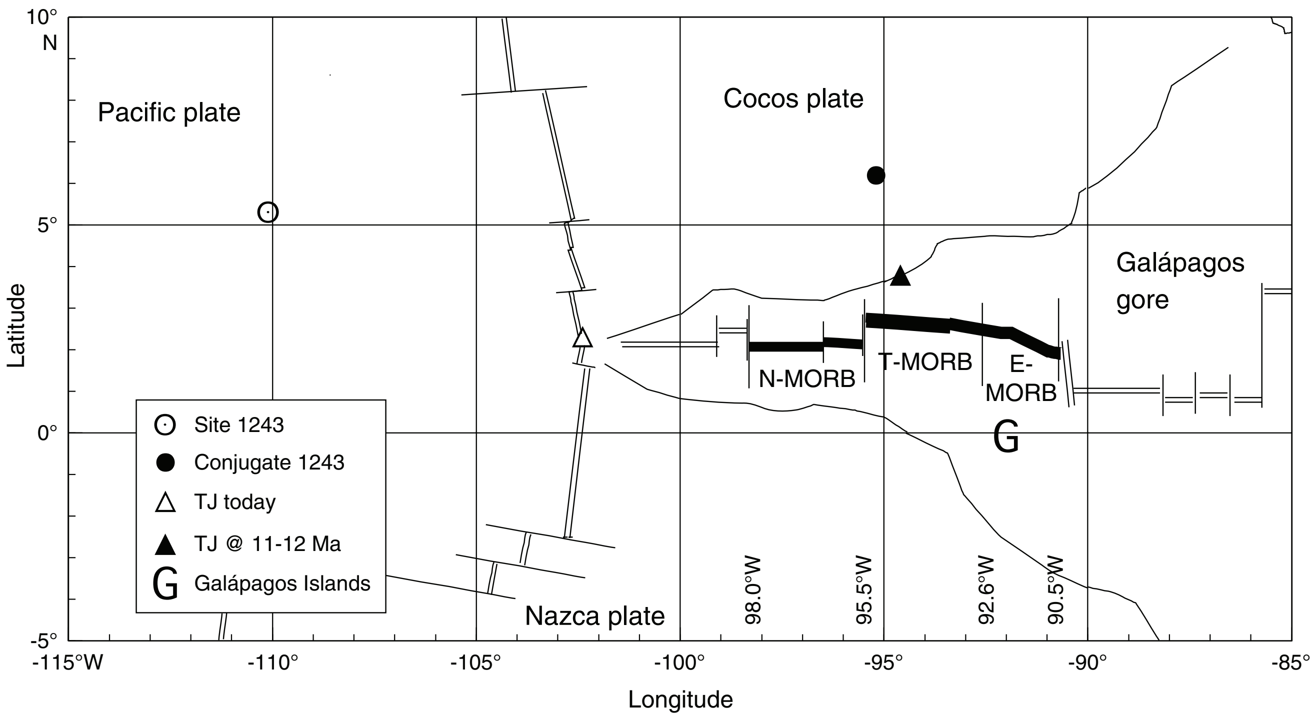

Table T1. Basaltic glass composition.

Identification	Geochemical group	Element oxides (wt%)											
		SiO_2	TiO_2	Al_2O_3	Fe_{total}	MnO	MgO	CaO	Na_2O	K2O	P_2O_5	S	Total
RM_1H2		49.94	1.477	15.022	10.392	0.199	7.617	12.164	2.398	0.08	0.135	0.127	99.552
RM_1J1		50.26	1.46	15.119	10.207	0.178	7.466	12.204	2.483	0.082	0.118	0.119	99.696
RM2_G1		49.995	1.488	15.159	10.261	0.184	7.572	12.189	2.497	0.084	0.12	0.129	99.68
RM2_F2		50.006	1.478	15.195	10.156	0.198	7.611	12.151	2.501	0.09	0.111	0.122	99.619
RM3C4 ave		50.012	1.45	15.235	9.942	0.176	7.583	12.078	2.425	0.088	0.086	0.12	99.194
RM 4 H 1		50.12	1.477	15.113	10.271	0.193	7.633	12.285	2.417	0.082	0.114	0.136	99.839
RM_5_D9		50.058	1.501	14.919	10.344	0.2	7.632	12.065	2.496	0.082	0.091	0.127	99.514
RM_5_E3	H	50.203	1.458	14.98	10.352	0.191	7.671	12.091	2.489	0.086	0.105	0.124	99.751
RM_5_F6		50.956	1.486	14.275	10.476	0.189	7.704	12.314	2.481	0.086	0.122	0.122	100.21
RM_5_I_12		50.153	1.442	14.721	10.313	0.192	7.668	11.984	2.497	0.086	0.122	0.119	99.297
RM_5_H_2		50.674	1.453	14.896	10.27	0.163	7.695	12.041	2.479	0.089	0.13	0.128	100.019
KA2 B 3		50.722	1.492	14.892	10.421	0.186	7.542	12.15	2.506	0.087	0.131	0.127	100.255
KA3 J 5		50.197	1.44	15.087	10.169	0.189	7.638	12.194	2.465	0.085	0.106	0.126	99.697
KA3 H 7		50.355	1.457	15.091	10.098	0.185	7.658	12.206	2.452	0.085	0.119	0.131	99.835
KA3 G 9		50.277	1.453	15.146	10.268	0.187	7.671	12.113	2.541	0.081	0.124	0.123	99.983
19R2-16		50.628	1.482	14.614	9.904	0.145	7.594	12.337	2.539	0.082	0.135	0.134	99.909
RM_1I2		50.714	1.736	14.616	10.872	0.22	6.71	11.662	2.726	0.107	0.145	0.138	99.645
RM_1F4		50.381	1.73	14.335	11.285	0.227	6.89	11.589	2.582	0.107	0.148	0.143	99.418
RM_1C2		50.944	1.729	14.354	11.039	0.191	6.991	11.745	2.606	0.11	0.151	0.142	100.002
RM_1C3		50.889	1.688	14.548	10.843	0.192	7.068	11.76	2.561	0.108	0.147	0.147	99.949
RM_1A3		51.406	1.679	14.52	10.871	0.19	7.075	11.801	2.575	0.102	0.125	0.139	100.484
RM_1B2		50.816	1.709	14.507	10.912	0.193	7.089	11.833	2.561	0.102	0.122	0.134	99.978
RM_1D2		50.923	1.692	14.367	10.923	0.192	7.118	11.775	2.541	0.099	0.154	0.134	99.916
RM_1H3		50.076	1.756	14.721	10.978	0.209	7.124	11.639	2.649	0.098	0.15	0.14	99.541
RM_1C1		50.135	1.743	14.821	10.866	0.204	7.128	11.643	2.671	0.096	0.158	0.13	99.596
RM_1D3		51.179	1.668	14.429	10.782	0.204	7.138	11.835	2.516	0.093	0.155	0.13	100.128
RM_1G3		50.138	1.677	14.519	10.875	0.206	7.14	11.81	2.525	0.102	0.142	0.141	99.275
RM_1E1		50.911	1.668	14.396	10.788	0.189	7.14	11.867	2.511	0.104	0.149	0.14	99.861
RM_1C4		50.732	1.687	14.513	10.825	0.195	7.143	11.879	2.539	0.103	0.123	0.142	99.881
RM_1E3		51.13	1.673	14.323	10.775	0.191	7.143	11.889	2.504	0.106	0.138	0.142	100.013
RM_1A2		50.407	1.677	14.542	10.748	0.189	7.145	11.799	2.559	0.097	0.131	0.138	99.431
RM_1E2		50.704	1.76	14.677	10.827	0.214	7.148	11.638	2.645	0.103	0.148	0.14	100.004
RM_1F2		50.413	1.657	14.469	10.843	0.217	7.151	11.889	2.502	0.099	0.13	0.139	99.507
RM_1G2		50.162	1.783	14.767	10.847	0.216	7.152	11.674	2.638	0.105	0.155	0.137	99.637
RM_1F3		51.029	1.648	14.435	10.79	0.19	7.156	11.816	2.495	0.099	0.132	0.139	99.929
RM_1F1		50.56	1.655	14.458	10.86	0.202	7.176	11.855	2.532	0.099	0.128	0.138	99.661
RM_1H1		50.355	1.674	14.479	10.911	0.195	7.184	11.803	2.52	0.104	0.156	0.137	99.517
RM_1H4		50.412	1.675	14.413	10.826	0.192	7.186	11.829	2.514	0.109	0.126	0.137	99.42
RM2_I2		50.313	1.75	14.37	11.014	0.199	7.013	11.714	2.689	0.097	0.174	0.131	99.464
RM_1J3	M	50.008	1.741	14.99	10.747	0.182	7.032	11.642	2.766	0.101	0.166	0.133	99.509
RM2_A4		50.049	1.752	14.908	10.697	0.182	7.048	11.646	2.774	0.108	0.151	0.142	99.457
RM_1I3		50.43	1.686	14.598	10.835	0.182	7.061	11.771	2.659	0.094	0.123	0.127	99.567
RM_1J4		49.925	1.752	15.084	10.854	0.201	7.061	11.659	2.816	0.103	0.156	0.14	99.752
RM2_I3		50.176	1.774	14.397	11.031	0.203	7.064	11.706	2.707	0.106	0.149	0.135	99.431
RM_1I4		50.484	1.696	14.677	10.752	0.231	7.073	11.822	2.67	0.091	0.134	0.136	99.765
RM2_A3		50.457	1.67	14.635	10.633	0.178	7.093	11.84	2.611	0.105	0.124	0.127	99.474
RM_1J2		50.544	1.655	14.624	10.67	0.199	7.098	11.875	2.64	0.095	0.137	0.131	99.667
RM2_E1		50.442	1.688	14.487	10.822	0.191	7.108	11.812	2.643	0.101	0.154	0.132	99.58
RM2_H4		50.352	1.674	14.615	10.764	0.185	7.108	11.863	2.643	0.103	0.146	0.139	99.592
RM2J2		49.855	1.752	14.836	10.881	0.201	7.117	11.66	2.77	0.098	0.155	0.135	99.46
RM2_D1		49.91	1.761	14.953	10.783	0.211	7.118	11.661	2.779	0.106	0.137	0.133	99.553
RM2J4		50.489	1.681	14.584	10.669	0.201	7.134	11.859	2.637	0.1	0.124	0.133	99.611
RM2_H3		49.751	1.766	14.943	10.82	0.208	7.155	11.685	2.819	0.113	0.148	0.131	99.539
RM2_G2		50.043	1.661	14.621	10.816	0.196	7.157	11.927	2.611	0.096	0.147	0.135	99.411
RM2_G3		50.164	1.674	14.638	10.786	0.184	7.163	11.82	2.648	0.111	0.132	0.13	99.451
RM2J3		50.02	1.663	14.64	10.915	0.191	7.168	11.848	2.66	0.104	0.154	0.126	99.488
RM2J1		49.984	1.674	14.536	10.827	0.206	7.181	11.802	2.639	0.104	0.122	0.132	99.206
RM3D5 ave		50.526	1.712	14.423	10.643	0.199	6.99	11.593	2.574	0.1	0.13	0.126	99.017
RM3F2 ave		50.61	1.702	14.754	10.714	0.193	6.997	11.597	2.603	0.104	0.118	0.137	99.529
RM3C2 ave		50.302	1.708	14.457	10.783	0.195	7.007	11.577	2.598	0.101	0.138	0.128	98.995
RM3E5 ave		51.001	1.658	14.605	10.537	0.212	7.048	11.687	2.579	0.104	0.136	0.136	99.704
RM3G2 ave		51.359	1.648	15.058	10.423	0.188	7.048	11.716	2.552	0.107	0.132	0.13	100.361
RM3B3 ave		50.288	1.723	14.93	10.543	0.19	7.091	11.577	2.73	0.104	0.144	0.13	99.45
RM3C3 ave		50.592	1.657	14.668	10.416	0.19	7.091	11.673	2.543	0.103	0.114	0.13	99.176

Notes: Microprobe analyses performed at School of Ocean and Earth Sciences and Technology, University of Hawaii. Identification is the location of randomly sampled chips in the plastic mounts. Most values are the arithmetic mean of four analyses per chip. * = three analyses per chip. Only a portion of this table appears here. The complete table is available in **ASCII.**

Table T2. Thin section analyses.

Core, section (piece, cm)	Lithologic unit/ Analysis	Element oxides (wt%)											
		SiO_2	TiO_2	Al_2O_3	Fe_{total}	MnO	MgO	CaO	Na_2O	K_2O	P_2O_5	S	Total
203-1243B-													
4R-1 (7, 55.5)	3/1	51.05	1.73	14.37	10.11	0.17	7.12	12.05	2.87	0.17	0.16	0.13	99.92
4R-2 (17, 122)	3/2	51.09	1.73	14.54	10.13	0.18	7.24	12.12	2.79	0.16	0.16	0.13	100.28
8R-1 (18, 125)	4/1	50.08	2.22	15.78	9.28	0.15	6.42	10.41	3.49	0.75	0.32	0.12	99.03
9R-1 (4, 37.5)	4/2	50.11	2.26	16.55	9.50	0.16	6.18	10.46	3.61	0.78	0.38		
10R-1 (1, 0.0)	4/3	50.09	2.30	16.54	9.42	0.16	6.26	10.40	3.61	0.78	0.36		
11R-1 (3, 11.0)	5/1	51.22	1.95	14.39	10.58	0.18	7.15	11.58	2.90	0.19	0.17	0.14	100.47

Note: Microprobe analyses performed at School of Ocean and Earth Sciences and Technology, University of Hawaii. Lithologic units determined on board ship (Shipboard Scientific Party, 2003a).

Table T3. Raw microprobe data. (See table note. Continued on next three pages.)

Lithologic unit	Depth (mbsf)	Element oxides (wt%)										
		SiO_2	TiO_2	Al_2O_3	Fe_{total}	MnO	MgO	CaO	Na_2O	K_2O	P_2O_5	Total
U3	113.27	49.874	1.732	14.434	9.768	0.159	7.07	11.84	3.174	0.167	0.197	98.446
		49.408	1.793	14.516	10.158	0.185	7.056	11.833	2.911	0.169	0.165	98.228
		50.112	1.82	14.464	10.556	0.168	7.199	11.839	3.017	0.145	0.193	99.664
		49.929	1.788	14.422	10.27	0.155	7.041	11.557	3.14	0.166	0.185	98.826
		49.747	1.691	14.374	9.604	0.218	6.761	11.371	2.958	0.182	0.171	97.108
		49.747	1.838	14.017	9.884	0.214	6.866	11.321	3.163	0.187	0.178	97.538
		49.63	1.866	14.114	9.737	0.15	7.021	11.73	3.177	0.199	0.153	97.894
		49.868	1.877	14.203	9.721	0.127	6.887	11.777	2.845	0.18	0.209	97.768
		49.269	1.67	14.532	9.876	0.173	7.12	11.602	3.081	0.192	0.187	97.839
		50.306	1.893	14.397	10.026	0.218	6.863	11.836	2.863	0.175	0.194	98.87
	119.46	49.822	1.689	14.444	9.811	0.188	7.154	11.772	2.997	0.159	0.197	98.458
		49.414	1.828	14.072	9.715	0.212	7.234	12.007	3.058	0.177	0.176	97.975
		50.022	1.741	14.429	10.201	0.174	7.151	11.871	2.837	0.167	0.187	98.926
		49.69	1.744	14.193	10.166	0.176	7.018	11.783	3.125	0.176	0.186	98.35
		49.95	1.718	14.421	10.458	0.18	7.117	11.833	3.073	0.162	0.192	99.211
		49.759	1.726	14.384	9.602	0.225	7.08	11.34	3.117	0.159	0.187	97.724
		50.091	1.694	14.181	10.456	0.218	6.779	11.878	3.122	0.159	0.179	98.889
		49.283	1.694	14.358	9.962	0.185	7.015	11.739	3.029	0.177	0.182	97.682
		49.778	1.814	14.507	10.11	0.232	7.237	11.411	3.022	0.156	0.197	98.522
		49.392	1.704	14.542	10.218	0.168	7.098	11.715	3.083	0.162	0.186	98.375
	119.65	49.744	1.702	14.146	9.457	0.184	7.164	11.119	2.873	0.166	0.166	96.894
		49.661	1.819	14.117	9.664	0.174	6.968	11.513	3.064	0.19	0.189	97.487
		49.302	1.727	14.007	10.154	0.197	7.086	11.478	3.014	0.164	0.174	97.399
		49.121	1.82	14.239	10.13	0.173	7.038	11.261	3.084	0.168	0.196	97.33
		49.539	1.782	14.163	9.548	0.193	7.129	11.638	3.117	0.18	0.187	97.594
		49.96	1.738	14.192	9.745	0.24	6.948	11.666	3.056	0.154	0.181	98.009
		49.837	1.822	14.24	10.051	0.154	7.068	11.592	3.041	0.176	0.18	98.311
		49.334	1.793	14.027	10.231	0.26	7.188	11.446	3.161	0.169	0.176	97.958
		50.239	1.814	14.478	9.938	0.205	7.128	11.612	3.04	0.17	0.172	98.915
		50.192	1.736	14.229	9.298	0.187	7.058	11.73	3.026	0.199	0.184	97.988
	128.01	49.903	1.677	14.542	10.468	0.205	7.256	11.688	3.022	0.154	0.186	99.268
		49.763	1.689	14.125	9.892	0.17	6.608	11.024	3.073	0.191	0.188	96.893
		49.37	1.778	14.489	9.722	0.185	7.156	11.744	2.938	0.161	0.182	97.847
		49.615	1.785	14.3	10.031	0.178	7.109	11.613	3.078	0.169	0.178	98.216
		49.992	1.782	14.496	10.432	0.201	7.045	11.772	3.066	0.162	0.213	99.239
		50.353	1.748	14.643	10.591	0.162	7.207	11.731	1.955	0.159	0.187	98.9
		50.27	1.699	14.569	10.056	0.182	7.261	11.779	3.189	0.177	0.149	99.422
		49.661	1.71	14.402	9.902	0.212	7.269	11.815	3.004	0.165	0.144	98.457
		50.279	1.724	14.626	9.746	0.2	7.274	11.856	3.128	0.164	0.214	99.363
		49.2	1.743	14.384	10.153	0.18	7.341	11.495	3.066	0.168	0.18	97.961
	128.17	50.04	1.811	14.752	10.012	0.208	7.184	11.496	3.05	0.167	0.169	99.075
		49.627	1.702	14.21	9.749	0.166	6.953	11.816	3.087	0.158	0.182	97.831
		49.815	1.725	14.471	10.433	0.217	7.204	11.796	3.037	0.197	0.199	99.177
		49.857	1.683	14.551	10.098	0.193	6.922	11.71	3.049	0.175	0.203	98.573
		49.904	1.772	14.542	9.728	0.204	7.107	11.787	3.085	0.162	0.169	98.558
		49.971	1.734	14.368	10.055	0.217	7.284	11.413	3.093	0.157	0.173	98.652
		50.184	1.792	14.985	9.967	0.204	7.39	12.081	3.098	0.168	0.181	100.259
		50.104	1.696	14.52	10.317	0.225	7.094	11.791	2.973	0.15	0.172	99.258
		49.99	1.833	14.36	10.064	0.192	7.181	11.691	2.92	0.151	0.166	98.661
		49.142	1.69	14.431	9.834	0.188	7.028	11.012	2.998	0.175	0.183	96.845
	129.08	49.43	1.808	14.205	10.12	0.177	6.979	11.79	2.984	0.148	0.173	97.935
		49.782	1.799	14.554	10.025	0.189	6.92	11.694	3.01	0.203	0.171	98.513
		49.583	1.828	14.523	10.071	0.196	7.22	11.656	3.13	0.144	0.169	98.653
		50.109	1.734	14.614	10.297	0.217	7.2	11.633	3.213	0.183	0.172	99.58
		50.679	1.729	14.678	10.288	0.138	7.217	11.259	3.177	0.156	0.174	99.63
		50.002	1.774	14.583	10.131	0.248	7.304	11.798	3.111	0.164	0.178	99.399
		49.821	1.733	14.464	10.259	0.213	7.345	11.893	3.066	0.15	0.191	99.231
		49.666	1.744	14.396	9.957	0.193	7.082	11.789	3.109	0.168	0.202	98.375
		49.983	1.712	14.598	10.319	0.237	7.209	11.714	3.135	0.171	0.168	99.34
		50.274	1.832	14.685	10.164	0.196	7.257	11.625	2.57	0.183	0.19	99.188
U4	138.99	49.17	2.201	15.877	9.482	0.152	6.288	10.431	3.585	0.736	0.4	98.346
		49.018	2.404	15.74	9.667	0.16	6.182	10.079	3.69	0.772	0.374	98.152
		49.096	2.405	16.005	8.663	0.187	6.335	10.2	3.667	0.68	0.381	97.72
		48.462	2.276	15.798	9.559	0.149	6.194	10.251	3.524	0.727	0.369	97.375
		49.103	2.281	15.654	8.89	0.136	6.289	10.265	3.711	0.795	0.359	97.665
		47.996	2.401	15.679	9.555	0.194	6.201	10.143	3.718	0.729	0.349	97.096
		48.91	2.134	15.795	9.548	0.17	6.498	10.053	3.823	0.725	0.398	98.139
		48.771	2.316	15.795	9.618	0.116	6.326	10.189	3.587	0.744	0.376	98.013
		48.88	2.234	15.937	9.277	0.188	6.307	10.146	3.836	0.749	0.409	98.01

Table T3 (continued).

Lithologic unit	Depth (mbsf)	Element oxides (wt%)										
		SiO_2	TiO_2	Al_2O_3	Fe_{total}	MnO	MgO	CaO	Na_2O	K_2O	P_2O_5	Total
		49.008	2.425	15.768	9.569	0.144	6.266	9.915	3.663	0.717	0.386	97.991
	139.51	48.426	2.393	15.876	9.706	0.167	6.23	10.113	3.599	0.738	0.378	97.746
		48.399	2.422	15.731	9.813	0.164	6.279	10.111	3.721	0.716	0.392	97.804
		48.275	2.193	15.277	9.71	0.147	6.099	9.893	3.52	0.7	0.38	96.339
		49.042	2.292	15.959	10.12	0.184	6.364	10.135	3.76	0.726	0.407	99.074
		49.27	2.236	15.881	9.599	0.196	6.44	10.32	3.631	0.739	0.351	98.777
		49.318	2.331	15.809	9.291	0.146	6.421	9.491	3.738	0.776	0.353	97.73
		49.248	2.261	16.013	9.741	0.181	6.464	10.208	3.755	0.71	0.371	99.05
		48.323	2.403	15.616	9.545	0.147	6.319	9.748	3.552	0.744	0.397	96.931
		49.676	2.279	16.339	9.681	0.203	6.477	10.417	3.757	0.675	0.378	99.938
		48.111	2.247	15.722	9.573	0.18	6.281	9.736	3.566	0.672	0.383	96.527
	139.55	48.042	2.248	15.559	9.786	0.166	6.177	9.792	3.653	0.732	0.394	96.612
		48.747	2.311	15.666	9.626	0.138	6.351	10.108	3.768	0.732	0.387	97.855
		48.625	2.321	15.71	9.621	0.143	6.145	9.636	3.473	0.752	0.357	96.885
		48.51	2.354	15.286	8.838	0.201	6.188	9.782	3.424	0.708	0.415	95.768
		48.312	2.305	15.563	9.495	0.18	6.245	10.075	3.523	0.745	0.385	96.932
		50.341	2.376	16.397	10.016	0.175	6.439	10.209	3.766	0.734	0.395	100.913
		49.479	2.471	15.905	9.527	0.163	6.305	10.191	3.681	0.768	0.402	99.1
		49.02	2.311	15.596	9.194	0.194	6.392	10.055	3.641	0.749	0.395	97.547
		48.904	2.154	15.362	9.341	0.179	6.306	10.275	3.689	0.721	0.395	97.364
		48.632	2.313	15.766	10.167	0.173	6.38	10.34	3.527	0.763	0.37	98.439
	143	49.27	2.22	15.753	9.636	0.182	6.26	10.23	3.428	0.734	0.393	98.247
		49.049	2.216	15.777	9.879	0.159	6.306	10.228	3.703	0.71	0.41	98.639
		48.439	2.439	15.462	9.315	0.204	6.398	10.254	3.472	0.705	0.418	97.173
		48.674	2.287	15.585	9.774	0.175	6.289	10.04	3.628	0.738	0.351	97.743
		48.633	2.255	15.709	9.654	0.161	6.377	9.899	3.681	0.709	0.342	97.446
		48.238	2.307	15.779	9.623	0.203	6.417	10.173	3.798	0.72	0.388	97.777
		48.843	2.245	15.854	9.538	0.155	6.077	10.238	3.568	0.728	0.405	97.733
		49.041	2.245	15.807	9.495	0.157	6.397	10.185	3.736	0.714	0.389	98.208
		49.029	2.194	15.737	9.694	0.21	6.425	10.169	3.712	0.727	0.38	98.385
		48.977	2.169	15.565	9.636	0.169	6.268	10.296	3.705	0.717	0.364	98.004
	143.22	48.325	2.325	15.527	9.407	0.237	6.367	10.236	3.809	0.73	0.364	97.367
		48.629	2.244	15.906	9.536	0.169	6.228	10.049	3.584	0.754	0.377	97.557
		48.344	2.27	15.708	9.526	0.152	6.288	10.162	3.6	0.71	0.413	97.249
		48.582	2.215	15.779	9.635	0.188	6.261	10.275	3.623	0.756	0.371	97.726
		48.569	2.261	15.925	9.56	0.177	6.377	10.091	3.507	0.756	0.379	97.714
		48.53	2.224	15.776	9.412	0.209	5.855	10.019	3.402	0.757	0.409	96.701
		48.718	2.235	15.363	9.549	0.155	6.458	10.33	3.501	0.764	0.34	97.516
		48.282	2.329	15.628	9.458	0.125	6.118	10.135	3.603	0.726	0.389	96.809
		48.487	2.2	15.62	9.316	0.162	6.257	10.138	3.667	0.756	0.379	97.049
		48.759	2.257	15.647	9.59	0.162	6.413	10.257	3.663	0.746	0.366	98.009
	143.27	49.932	2.199	15.815	9.147	0.17	6.461	10.123	3.703	0.744	0.42	98.794
		49.441	2.417	15.818	9.099	0.195	6.438	10.138	3.541	0.761	0.39	98.286
		49.245	2.232	15.528	8.977	0.165	6.372	9.487	3.458	0.805	0.356	96.714
		48.947	2.197	15.629	8.93	0.139	6.367	10.22	3.589	0.788	0.369	97.303
		49.036	2.208	15.601	9.294	0.204	6.327	9.979	3.823	0.793	0.38	97.816
		49.382	2.241	15.823	8.979	0.183	6.354	10.162	3.81	0.772	0.361	98.262
		48.942	2.432	15.561	9.511	0.202	6.291	10.19	3.744	0.81	0.409	98.193
		48.493	2.287	15.305	9.362	0.171	6.438	9.923	3.182	0.804	0.381	96.419
		49.076	2.177	15.716	9.305	0.144	6.476	10.166	3.409	0.737	0.413	97.694
		49.005	2.194	15.749	9.445	0.162	6.543	10.174	3.808	0.796	0.376	98.358
	143.46	48.708	2.265	15.703	8.936	0.205	6.487	9.691	3.688	0.773	0.347	96.926
		48.492	2.454	15.627	8.104	0.168	6.382	10.071	3.395	0.779	0.365	96.061
		49.24	2.292	15.561	8.442	0.172	6.518	10.215	3.621	0.725	0.388	97.273
		48.792	2.335	15.386	8.385	0.183	6.397	10.178	3.838	0.78	0.381	96.755
		49.155	2.238	15.594	8.491	0.19	6.511	10.29	3.619	0.785	0.36	97.418
		48.928	2.362	15.692	8.384	0.148	6.06	10.277	3.644	0.784	0.367	96.68
		48.894	2.427	15.791	8.207	0.207	6.547	10.247	3.789	0.739	0.371	97.269
		49.167	2.246	15.641	8.472	0.186	6.271	10.313	3.772	0.791	0.399	97.348
		48.438	2.337	15.647	8.486	0.153	6.255	10.255	3.775	0.762	0.371	96.552
		48.718	2.215	15.711	8.564	0.181	6.493	9.988	3.638	0.788	0.413	96.813
	143.7	48.914	2.172	15.621	8.396	0.191	6.411	9.896	3.672	0.764	0.384	96.565
		49.11	2.35	15.674	8.532	0.164	6.472	9.957	3.761	0.763	0.382	97.242
		48.89	2.364	15.604	8.551	0.14	6.527	10.033	3.663	0.772	0.373	96.987
		48.863	2.385	15.235	8.398	0.159	6.553	10.341	3.057	0.771	0.364	96.221
		48.555	2.302	15.456	8.628	0.184	6.595	10.379	3.654	0.747	0.392	96.997
		48.879	2.371	15.434	8.361	0.18	6.501	10.171	3.664	0.813	0.374	96.79
		48.971	2.431	15.055	8.59	0.096	6.497	9.982	3.699	0.748	0.367	96.636
		49.107	2.28	15.602	8.79	0.174	6.497	10.228	3.717	0.773	0.357	97.643

Table T3 (continued).

Lithologic unit	Depth (mbsf)	Element oxides (wt%)										
		SiO_2	TiO_2	Al_2O_3	Fe_{total}	MnO	MgO	CaO	Na_2O	K_2O	P_2O_5	Total
		48.397	2.262	15.508	8.793	0.168	6.448	10.107	3.537	0.773	0.39	96.547
		49.192	2.329	15.612	8.487	0.133	6.452	10.298	3.837	0.775	0.356	97.602
	147	48.928	2.261	15.672	8.624	0.193	6.419	10.12	3.763	0.779	0.355	97.332
		49.282	2.389	15.612	8.673	0.192	6.538	10.07	3.787	0.814	0.378	97.8
		49.139	2.361	15.652	8.693	0.179	6.478	10.109	3.592	0.775	0.356	97.541
		49.45	2.255	15.597	8.364	0.193	6.5	10.194	3.712	0.719	0.39	97.427
		49.292	2.186	15.652	8.794	0.142	6.544	9.867	3.57	0.731	0.366	97.255
		49.348	2.236	15.615	9.044	0.172	6.572	10.157	3.836	0.759	0.355	98.212
		48.994	2.379	15.516	8.735	0.176	6.413	10.396	3.632	0.82	0.369	97.472
		49.023	2.31	15.519	8.787	0.135	6.51	10.21	3.682	0.715	0.389	97.395
		49.072	2.459	15.679	8.578	0.15	6.571	10.179	3.722	0.777	0.34	97.637
		49.152	2.22	15.642	8.58	0.142	6.561	10.148	3.338	0.749	0.391	97.1
	147.05	49.191	2.289	15.59	8.415	0.178	6.386	9.941	3.769	0.795	0.411	97.092
		49.035	2.365	15.617	9.469	0.225	6.465	9.847	3.653	0.783	0.348	97.937
		49.128	2.253	15.512	9.317	0.195	6.537	10.071	3.766	0.769	0.38	98.047
		48.598	2.252	15.629	9.206	0.2	6.344	10.096	3.042	0.741	0.387	96.674
		49.2	2.264	15.575	9.323	0.178	6.503	10.116	3.737	0.795	0.393	98.099
		48.8	2.243	15.664	9.392	0.184	6.33	10.04	3.79	0.744	0.371	97.762
		48.998	2.291	15.619	9.187	0.202	6.409	10.176	3.768	0.731	0.369	97.868
		48.744	2.202	15.521	9.532	0.166	6.214	10.03	3.71	0.753	0.396	97.456
		48.587	2.438	15.656	9.236	0.206	6.459	10.146	3.737	0.747	0.359	97.7
		48.928	2.296	15.484	9.644	0.158	6.153	9.889	3.583	0.743	0.405	97.314
	147.4	49.185	2.351	15.586	9.208	0.187	6.54	10.229	3.735	0.785	0.372	98.283
		48.83	2.371	15.735	9.428	0.141	6.206	10.041	3.804	0.768	0.397	97.885
		48.806	2.209	15.585	9.149	0.206	6.496	9.459	3.672	0.741	0.374	96.736
		49.097	2.227	15.483	9.096	0.164	6.513	10.095	3.404	0.784	0.356	97.394
		49.027	2.184	15.335	9.109	0.205	6.474	10.124	3.737	0.754	0.382	97.402
		49.17	2.226	15.793	9.524	0.168	6.335	10.379	3.682	0.771	0.379	98.511
		49.207	2.417	15.751	9.346	0.214	6.341	10.239	3.893	0.764	0.362	98.659
		49.124	2.307	15.643	9.239	0.186	6.515	10.169	3.611	0.778	0.401	98.129
		48.978	2.454	15.749	9.049	0.193	6.537	10.185	3.411	0.805	0.361	97.914
		48.774	2.278	15.623	8.538	0.157	6.49	10.234	3.478	0.775	0.371	96.788
	151.51	49.118	2.361	15.638	9.537	0.177	6.531	10.134	3.611	0.788	0.398	98.451
		49.415	2.332	15.669	9.322	0.172	6.383	10.268	3.166	0.783	0.386	98.029
		49.277	2.237	15.674	9.233	0.153	6.404	10.087	3.612	0.773	0.421	97.884
		49.126	2.411	15.695	9.215	0.165	6.241	10.019	3.479	0.772	0.348	97.619
		48.859	2.273	15.615	9.643	0.143	6.543	10.034	3.536	0.78	0.374	97.945
		49.042	2.285	15.345	9.195	0.175	6.502	10.162	3.287	0.791	0.384	97.329
		49.282	2.344	15.499	8.732	0.163	6.427	10.059	3.711	0.786	0.376	97.445
		48.862	2.237	15.606	9.367	0.197	6.367	9.427	3.615	0.763	0.36	96.911
		49.132	2.288	15.737	9.337	0.207	6.188	10.142	3.706	0.764	0.365	98.013
		49.042	2.32	15.728	9.435	0.2	6.52	10.245	3.714	0.808	0.34	98.573
	151.55	49.329	2.259	15.787	9.301	0.186	6.342	10.26	3.657	0.783	0.356	98.305
		48.752	2.364	15.572	9.235	0.177	6.347	9.815	3.64	0.775	0.373	97.075
		49.075	2.296	15.784	9.38	0.142	6.343	10.24	3.716	0.799	0.364	98.214
		48.78	2.214	15.9	9.423	0.199	6.316	9.987	3.767	0.774	0.384	97.886
		48.846	2.383	15.566	9.435	0.164	6.289	10.169	3.553	0.775	0.358	97.684
		49.336	2.321	15.901	9.386	0.177	6.359	9.925	3.592	0.776	0.388	98.256
		49.058	2.255	15.746	8.353	0.147	6.299	9.937	3.572	0.792	0.349	96.63
		48.769	2.203	15.586	9.296	0.245	6.151	10.219	3.611	0.802	0.377	97.407
		49.156	2.294	16.013	8.912	0.185	6.212	10.281	3.725	0.737	0.367	98.027
		48.938	2.244	15.87	9.297	0.198	6.447	9.842	3.623	0.754	0.383	97.716
U5	156.61	49.57	2.096	13.976	9.596	0.192	7.249	10.891	2.953	0.191	0.208	97.018
		49.842	2.02	14.071	9.506	0.215	7.274	11.485	3.036	0.227	0.213	97.995
		49.782	2.044	14.099	9.826	0.226	7.212	11.178	3.045	0.183	0.202	98.041
		49.596	1.997	14.129	9.851	0.182	6.953	11.272	3.053	0.202	0.197	97.577
		49.87	2.02	14.07	9.712	0.201	6.999	11.222	3.053	0.226	0.211	97.738
U6Na	160.7	49.856	2.701	14.048	11.156	0.213	5.098	9.896	4.657	0.471	0.457	98.645
U6&8K	166.65	49.549	3.192	13.588	12.74	0.262	5.201	9.383	3.507	0.631	0.455	98.572
	166.97	49.478	3.068	13.671	12.673	0.155	5.009	9.417	3.545	0.618	0.451	98.096
	167.02	49.975	3.17	13.891	12.502	0.2	5.099	8.89	3.674	0.633	0.472	98.625
	190.67	49.798	3.138	13.659	12.401	0.2	4.996	9.242	3.577	0.638	0.461	98.23
U6a	172.13	50.053	1.762	14.163	10.373	0.205	7.363	11.608	2.915	0.102	0.128	98.885
		49.188	1.752	14.1	9.327	0.205	7.637	11.429	2.925	0.099	0.129	96.878
		49.264	1.722	14.094	9.595	0.203	7.591	11.484	2.892	0.135	0.141	97.183
		49.313	1.696	14.118	9.816	0.199	7.263	11.485	2.966	0.119	0.162	97.314
		49.38	1.804	14.186	9.519	0.197	7.372	11.142	2.982	0.121	0.16	96.978
U8a	190.43	49.6	1.551	14.535	9.135	0.197	7.8	11.591	2.7	0.064	0.12	97.337
		49.285	1.497	14.514	9.486	0.224	8.023	12.25	2.544	0.091	0.11	98.163

Table T3 (continued).

Lithologic unit	Depth (mbsf)	Element oxides (wt%)										
		SiO_2	TiO_2	Al_2O_3	Fe_{total}	MnO	MgO	CaO	Na_2O	K_2O	P_2O_5	Total
		49.53	1.549	14.189	9.056	0.183	8.071	12.037	2.635	0.082	0.095	97.545
		49.527	1.648	14.484	9.132	0.228	7.758	11.521	2.65	0.105	0.125	97.356
		49.732	1.483	14.404	9.269	0.203	7.958	12.176	2.674	0.105	0.108	98.203
	190.49	49.935	1.527	14.68	10.156	0.156	8.121	12.038	2.992	0.068	0.094	99.84

Note: Microprobe analyses performed at Ocean Research Institute, University of Tokyo.

Table T4. Geochemical group composition averages.

Group	Characteristic	N	Element oxides (wt%)											
			SiO_2	TiO_2	Al_2O_3	Fe_{total}	MnO	MgO	CaO	Na_2O	K_2O	P_2O_5	S	Total
H	High Mg	16	50.325	1.466	14.936	10.245	0.184	7.626	12.159	2.476	0.084	0.117	0.126	99.768
M	Main	299	50.496	1.713	14.593	10.78	0.195	7.142	11.727	2.657	0.103	0.144	0.133	99.708
A	Above	55	50.411	1.951	14.683	10.77	0.195	6.782	11.377	2.882	0.201	0.19	0.132	99.584
B	Below	24	50.557	1.94	13.899	11.878	0.211	6.597	11.359	2.752	0.108	0.16	0.151	99.64
K	High K	188	50.325	2.999	14.042	12.851	0.226	4.82	9.398	3.526	0.644	0.396	0.162	99.414

Note: N = number of samples.

Table T5. Basalt composition averages.

MORB type	Element oxides (wt%)								
	SiO_2	TiO_2	Al_2O_3	Fe_{total}	MgO	CaO	Na_2O	K_2O	P_2O_5
Normal	50.53	1.56	15.27	10.46	7.47	11.49	2.62	0.18	0.13
Enriched	49.98	1.99	15.11	11.04	6.87	11.25	2.81	0.47	0.32

Notes: Data from McBirney, 1993. MORB = mid-ocean-ridge basalt.

Table T6. Shipboard ICP-AES analyses.

Lithologic unit/ Analysis	Depth (mbsf)	Element oxides (wt%)										
		SiO_2	TiO_2	Al_2O_3	Fe_{total}	MnO	MgO	CaO	Na_2O	K_2O	P_2O_5	Total
1	108.8	50.05	1.69	15.15	9.74	0.18	7.26	12.57	3.05	0.3	0.12	100.11
3-1	114.4	50.81	1.67	15.49	10.25	0.17	6.44	12.15	2.95	0.14	0.19	100.26
3-2	124.3	50.12	1.68	15.28	10.09	0.18	6.5	12.5	3.01	0.39	0.15	99.9
3-3	130.1	51.05	1.72	15.36	8.86	0.16	7.27	12	3.07	0.1	0.18	99.78
4-1	139.3	50.19	2.11	16.88	9.23	0.15	5.91	10.64	3.56	0.78	0.32	99.76
4-2	149.8	49.78	2.14	16.86	9.51	0.15	5.78	11.81	3.44	0.76	0.36	100.57
5	157.1	51.72	1.98	15.27	9.63	0.17	6.12	11.68	3.05	0.32	0.21	100.16
7	176.7	52.1	2.02	15.01	14.29	0.17	6.17	11.4	3.07	0.27	0.18	104.68
8	190.4	50.91	1.48	15.79	12.53	0.18	6.75	12.54	2.56	0.15	0.11	103

Note: Lithologic units determined on board ship (Shipboard Scientific Party, 2003a).